

# Influence of vegetation on occurrence and time distributions of regional new aerosol particle formation and growth

Imre SALMA<sup>1,2</sup>, Wanda THÉN<sup>1,3</sup>, Pasi AALTO<sup>4</sup>, Veli-Matti KERMINEN<sup>4</sup>, Anikó KERN<sup>5</sup>, Zoltán BARCZA<sup>2,6,7</sup>, Tuukka PETÄJÄ<sup>4</sup>, and Markku KULMALA<sup>4</sup>

<sup>1</sup> Institute of Chemistry, Eötvös University, Budapest, Hungary

<sup>2</sup> Excellence Center, Faculty of Science, Eötvös University, Martonvásár, Hungary

<sup>3</sup> Hevesy György Ph. D. School of Chemistry, Eötvös University, Budapest, Hungary

<sup>4</sup> Institute for Atmospheric and Earth System Research, University of Helsinki, Helsinki, Finland

<sup>5</sup> Department of Geophysics and Space Science, Eötvös University, Budapest, Hungary

<sup>6</sup> Department of Meteorology, Eötvös University, Budapest, Hungary

<sup>7</sup> Faculty of Forestry and Wood Sciences, Czech University of Life Sciences, Prague, Czech Republic

Correspondence to: Imre Salma (salma@chem.elte.hu)

**Abstract.** Occurrence frequency ( $f_{\text{NPF}}$ ) of regional atmospheric new aerosol particle formation (NPF) and consecutive growth events were studied with respect to vegetation activity, aerosol properties, air pollutants and meteorological data in Budapest over the time interval of 2008–2018. The data set evaluated contained results of in situ measurements on land surface mostly performed at the Budapest platform for Aerosol Research and Training Laboratory, of satellite-based products recorded by MODIS on Terra and of modelled vegetation emission-related properties from an advanced regional biogeochemical model. Annual mean relative occurrence frequencies were considerable (with an overall mean of 21 %), remained at a constant level (with an overall SD of 5 %) and did not exhibit tendentious change over the years. The shape of the distributions of monthly mean  $f_{\text{NPF}}$  exhibited large variability from year to year, while the overall average distribution already possessed a characteristic pattern. The structure of the NPF occurrence distributions was compared to those of environmental variables including concentrations of gas-phase  $\text{H}_2\text{SO}_4$ ,  $\text{SO}_2$ ,  $\text{O}_3$ ,  $\text{NO}$ ,  $\text{NO}_2$ ,  $\text{CO}$ ,  $\text{PM}_{10}$  mass and  $\text{NH}_3$ , of particle numbers in the size fractions of 6–1000, 6–100 and 100–1000 nm, condensation sink, air temperature ( $T$ ), relative humidity, wind speed (WS), atmospheric pressure, global solar radiation, gross primary production of vegetation, leaf area index and stomatal conductance. There were no evident systematic similarities between  $f_{\text{NPF}}$  on one hand and all variables on the other hand, except for  $\text{H}_2\text{SO}_4$  and perhaps  $\text{NH}_3$ . The spring maximum in the NPF occurrence frequency distribution often overlapped with the time intervals of positive  $T$  anomaly on vegetated territories. The link between the potential heat stress exerted on plants in sultry summer intervals and the summer  $f_{\text{NPF}}$  minimum could not be proved. The relevance of environmental variables was assessed by their ratios on NPF event day and on non-event days. Gas-phase  $\text{H}_2\text{SO}_4$  concentration showed the largest monthly ratios, followed by  $\text{O}_3$ . The

36 WS, biogenic precursor gases and SO<sub>2</sub> can generally favour NPF events although their  
37 influence seemed to be constrained. Association between the  $f_{\text{NPF}}$  and vegetation growth  
38 dynamics was clearly identified.

## 39 **1 Introduction and objectives**

40 New aerosol particle formation (NPF) from atmospheric vapours and consecutive particle  
41 diameter growth events (Kulmala et al., 2014) were observed in all major continental  
42 environments in the world (e.g. Kerminen et al., 2018; Nieminen et al., 2018 and references  
43 therein). Their relevance for global aerosol burden, climate system and health risk issues are  
44 increasingly recognised (Spracklen et al., 2006; Makkonen et al., 2009, 2012; Merikanto et al.,  
45 2009; Yue et al., 2010; Sihto et al., 2011; Kerminen et al., 2012; Carslaw et al., 2013; Braakhuis  
46 et al., 2014; Salma et al., 2015; Dunne et al., 2016; Gordon et al., 2016; Ohlwein et al., 2019).

47  
48 Occurrence of NPF events is one of the fundamental properties of the phenomenon. The main  
49 circumstances influencing the regional NPF occurrence involve atmospheric chemical  
50 composition together with concentration and size distribution of aerosol particles,  
51 photochemical processes and meteorological properties (Kulmala et al., 2014). Some precursor  
52 compounds and their oxidation products such as SO<sub>2</sub> and H<sub>2</sub>SO<sub>4</sub>, volatile organic compounds  
53 (VOCs) and ~~extremely low volatility organic compounds (ELVOCs)~~ or highly oxygenated  
54 molecules (HOMs), NH<sub>3</sub> or amines, iodine oxides and HIO<sub>3</sub> were shown to influence NPF  
55 events (O'Dowd et al., 2002; Sipilä et al., 2010, 2016; Metzger et al., 2010; Kirkby et al., 2011,  
56 2016; Riipinen et al., 2011; Almeida et al., 2013; Donahue et al., 2013; Schobesberger et al.,  
57 2013; Ehn et al., 2014; Riccobono et al., 2014; Jokinen et al., 2015; Bianchi et al., 2016; Tröstl  
58 et al., 2016; Yao et al., 2018; Kürten, 2019; He et al., 2021). Further chemical species such as  
59 isoprene or NO<sub>2</sub> showed inhibiting effects (Kiendler-Scharr et al., 2009; Lehtipalo et al., 2016;  
60 Heinritzi et al., 2020; Simon et al., 2020). It was pointed out that NPF can proceed from HOMs  
61 alone when it is assisted by air ions (Kirkby et al., 2016). These conclusions were derived  
62 mostly from environmental or plant atmosphere chamber experiments. Meteorological  
63 parameters such as solar radiation, air temperature ( $T$ ), water vapour content or relative  
64 humidity (RH), wind speed (WS), boundary mixing layer height can also favour or depress  
65 NPF events (Birmili and Wiedensohler 2000; Hamed et al., 2011; Hirsikko et al., 2012; Jun et  
66 al., 2014; Dada et al., 2017). The actual occurrence may also be associated with some limiting  
67 or triggering atmospheric processes in the region (Manninen et al., 2010; Dall'Osto et al., 2013).

68 Galactic cosmic rays do not seem to contribute extensively to the overall nucleation under  
69 ordinary environmental conditions (e.g. in the presence of atmospheric chemical bases or  
70 HOMs) and particularly in the lower troposphere (Kirkby et al., 2011; 2016; Almeida et al.,  
71 2013; Riccobono et al., 2014; Dunne et al., 2016). As a consequence of all these factors, NPF  
72 events happen with a varying frequency in space and time.

73

74 The annual relative occurrence frequency of NPF events is typically between 10 % and 40 %  
75 for many geographical regions (Brines et al., 2015; Xiao et al., 2015; Kerminen et al., 2018;  
76 Nieminen et al., 2018; Bousiotis et al., 2019; Lee et al., 2019). The frequency changes  
77 substantially over a year since many multifactorial conditions and the complex interplay among  
78 the environmental variables influencing it have prominent seasonal variation (Tunved et al.,  
79 2006). Many studies reported spring or summer maximum (Qian et al., 2007; Wu et al., 2007;  
80 Meija and Morawska, 2009; Manninen et al., 2010; Salma et al., 2011; Vakkari et al., 2011;  
81 Hirsikko et al., 2012; Nieminen et al., 2014; Dall'Osto et al., 2018). This is, however, not  
82 universal, and the order of the seasons can vary among individual territories. Reliable  
83 experimental determination of the annual and monthly mean frequencies of regional NPF  
84 require long (semi-)continuous measurements since the occurrence can be influenced by inter-  
85 annual differences in chemical, aerosol and meteorological properties and in biogenic cycling.

86

87 It was also attempted to predict the distributions of the monthly mean occurrence frequency by  
88 combining the effects of environmental variables which can be derived from routine  
89 atmospheric measurements (e.g. Clement et al., 2001; Boy and Kulmala, 2002; Mikkonen et  
90 al., 2006). Conclusive prognostic or explanative methods could not be, however, achieved  
91 (Kerminen et al., 2018). This also means that the driving factors of NPF occurrence and their  
92 time variation have remained largely unidentified, poorly understood and unexplained. The  
93 lack of this knowledge and experimental information also hinders our understanding of the role  
94 of anthropogenic activities in related societal issues of aerosol particles such as their climate  
95 and health effects.

96

97 Several-year-long, semi-continuous, validated and complex atmospheric data set is available  
98 for the Budapest area. It has been studied and evaluated from several aspects. The major  
99 objectives of this study are 1) to determine and discuss the annual mean relative occurrence  
100 frequency and the distributions of monthly mean frequency of NPF events in Budapest for  
101 seven full measurement years in 2008–2018, 2) to investigate and explain the changes in the

102 shape of the distributions and their annual mean with respect to basic meteorological data,  
103 criteria air pollutants and other environmental factors including vegetation-related variables  
104 and 3) to evaluate and interpret the effects of vegetation on NPF occurrence together with the  
105 incidence between them. The involvement of the vegetation-related factors into the ambient  
106 NPF and their combination with the environmental influencing properties represent a  
107 noteworthy novelty in the research field. The present survey also prepares the full exploitation  
108 of the data base by advanced multi-variate statistical methods.

## 109 **2 Data sets**

110 The following environmental variables were considered in the study: number of NPF event  
111 days and non-event days, particle number concentrations in the diameter ranges from 6 to 1000  
112 nm ( $N$ ), from 6 to 100 nm ( $N_{6-100}$ ) and from 100 to 1000 nm ( $N_{100-1000}$ ), concentrations of gas-  
113 phase  $H_2SO_4$ ,  $SO_2$ ,  $O_3$ ,  $NO$ ,  $NO_x$ ,  $NO_2$ ,  $CO$ ,  $PM_{10}$  mass and  $NH_3$ , condensation sink (CS),  $T$ ,  
114 RH, WS, atmospheric pressure ( $P$ ), global solar radiation (GRad), gross primary production  
115 (GPP) of vegetation, leaf area index (LAI), stomatal conductance (SCT) and characteristics of  
116 vegetation growth dynamics such as start of spring (SoS) and green-up duration (GuD). Most  
117 variables were determined experimentally, while the variables ~~(last five properties)~~ related to  
118 vegetation (last five properties) were derived from an advanced regional biogeochemical model  
119 or from satellite-based vegetation products. The data sets actually evaluated in comparisons  
120 contained daily median atmospheric concentrations, daily means and standard deviations (SDs)  
121 for all variables and daily maximum values for GRad ( $GRad_{max}$ ). The individual data were  
122 averaged over each month, then separately for NPF event days and non-event day in each  
123 month, and finally over all measurement years in the city centre.

124  
125 The time intervals investigated comprise seven full measurement years, i.e. Y1) from 3  
126 November 2008 to 2 November 2009, Y2) from 19 January 2012 to 18 January 2013, Y3) from  
127 13 November 2013 to 12 November 2014, Y4) from 13 November 2014 to 12 November 2015,  
128 Y5) from 13 November 2015 to 12 November 2016, Y6) from 28 January 2017 to 27 January  
129 2018 and Y7) from 28 January 2018 to 27 January 2019. In Sect. 3.5, we also included the NPF  
130 occurrence data for the last full measurement year completed, i.e. from 28 January 2019 to 27  
131 January 2020 (Y8). Our specific purpose by adding this year was to improve the statistics in  
132 studying the effect of vegetation on NPF events. Local time (LT=UTC+1 or daylight-saving  
133 time, UTC+2) was chosen as the time base of the data because it had been observed that the

134 daily activity time pattern of inhabitants largely influences many atmospheric processes in  
135 cities (Salma et al., 2014; Sun et al., 2019; Mikkonen et al., 2020).

## 136 **2.1 Experimental data and their treatment**

137 The concentrations  $N$ ,  $N_{6-100}$  and  $N_{100-1000}$  were determined by a flow-switching type  
138 differential mobility particle sizer (DMPS; Salma et al., 2011, 2016b). Its main components  
139 include a radioactive ( $^{60}\text{Ni}$ ) bipolar charger, a Nafion semi-permeable membrane dryer, a 28-  
140 cm long Vienna-type differential mobility analyser and a condensation particle counter (TSI,  
141 model CPC3775). The measurements were performed in a diameter range from 6 to 1000 nm  
142 in the dry state of particles. The system was updated twice during the years, in spring 2013 and  
143 winter 2016. The major parts of the DMPS system were cleaned and serviced but remained  
144 unchanged. Extensive data validation, calibration or comparative exercises were realised in  
145 summer 2015 and in autumn 2019, which yielded acceptable results (Salma et al., 2016a;  
146 Mikkonen et al., 2020).

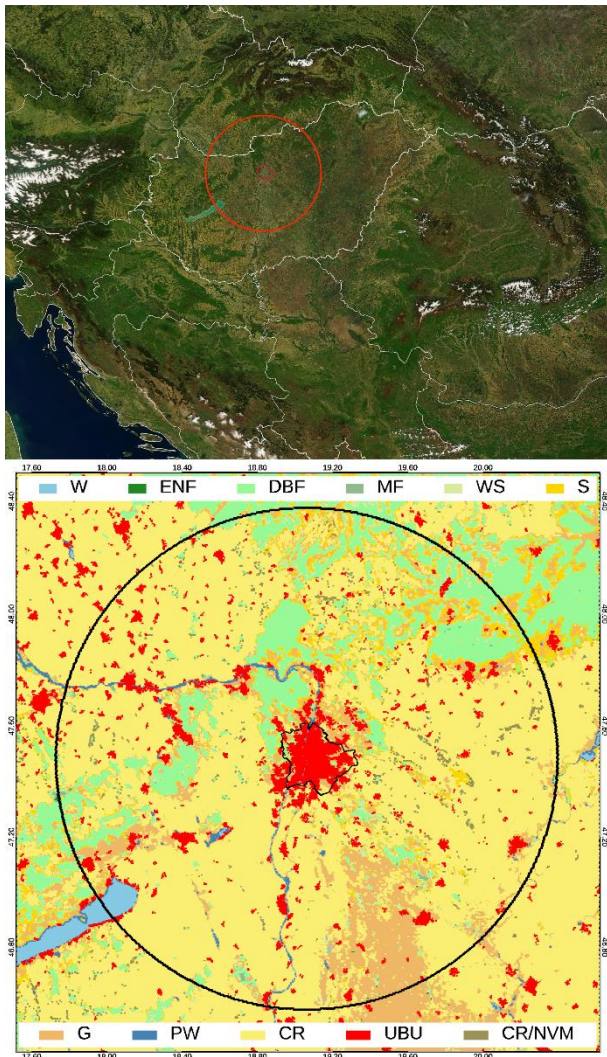
147

148 The DMPS data were used for identification and classification of the regional NPF events using  
149 daily particle number size distribution surface plots (Dal Maso et al., 2005; refined by Kulmala  
150 et al., 2012; Németh et al., 2018). The following main classes were separated: event days, non-  
151 event days, undefined days and days with missing data (for more than 4 h during the midday).  
152 Relative occurrence frequency of NPF events ( $f_{\text{NPF}}$ ) was determined for each month and year  
153 as the ratio of the number of event days to the total number of relevant days within the time  
154 interval dealt with. In order to evaluate the timing relationships between vegetation growth and  
155 NPF events (Sect. 3.5), the start of the NPF occurrence peak in spring (see later Fig. 2) had to  
156 be further refined. This was achieved by considering weekly time scale for determining the  
157 occurrence frequency. These data, however, showed larger scatter mainly due to the discrete  
158 daily character of NPF events. Therefore, the weekly occurrence frequency data sets for winter  
159 and spring were subjected to 1-month smoothing to derive less fluctuating time trends. The  
160 start of the NPF occurrence spring peak was set at the date (day of year) of the 20 %-value of  
161 the difference between the maximum smoothed spring peak frequency and the mean winter  
162 level of weekly frequencies (on the early side of the peak).

163

164 The DMPS measurements took place at two urban locations in Budapest, Hungary (Fig. 1). In  
165 the measurement year 2012–2013, they were performed in the near-city background, while in  
166 all other years, they were accomplished in the city centre. The former location is situated at the

167  
168  
169  
170  
171  
172  
173  
174  
175  
176  
177  
178  
179  
180  
181  
182  
183  
184  
185  
186  
187  
188  
189  
190



191 **Figure 1.** Location of Budapest in the Carpathian Basin and the circular geographical area with a radius of 100  
192 km around it, which was considered in modelling calculations (upper panel), and the spatial distribution of land  
193 cover types according to the International Geosphere-Biosphere Programme (IGBP) classification (lower panel). Both  
194 pictures were derived from satellite-based imagery data recorded by MODIS. W: water bodies, ENF: evergreen  
195 needleleaf forests, DBF: deciduous broadleaf forests, MF: mixed forests, WS: woody savannas, S: savannas, G:  
196 grasslands, PW: permanent wetlands, CR: croplands, UBU: urban and built-up lands, CR/NVM: cropland and  
197 natural vegetation mosaics.

198

199 NW border of Budapest in a wooded area of the Konkoly Astronomical Observatory (N 47°  
200 30' 00", E 18° 57' 47", 478 m above mean sea level, a.m.s.l.) of the Hungarian Academy of  
201 Sciences. This site characterises the air masses which enter the city since the prevailing wind  
202 direction in the area is NW. The measurements in the city centre were conducted at the  
203 Budapest platform for Aerosol Research and Training (BpART) Laboratory (N 47° 28' 30", E  
204 19° 3' 45", 115 m a.m.s.l.) of the Eötvös University (Salma et al., 2016a). It represents a well-  
205 mixed average atmospheric environment for the overall city centre.

206

207 The concentrations of SO<sub>2</sub>, O<sub>3</sub>, NO/NO<sub>x</sub>/NO<sub>2</sub>, CO and PM<sub>10</sub> mass were measured by UV  
208 fluorescence (Ysselbach 43C), UV absorption (Ysselbach 49C), chemiluminescence (Thermo  
209 42C), IR absorption (Thermo 48i) and beta-ray attenuation (Thermo FH62-I-R) methods,  
210 respectively with a time resolution of 1 h. The data were acquired from the closest measurement  
211 station of the National Air Quality Network in Budapest located in 4.5 km from the urban site,  
212 and of 6.9 km from the near-city background site in the ~~upwind~~-prevailing upwind direction  
213 (Salma and Németh, 2019).

214

215 It was previously shown that the NPF events observed in the Budapest ordinarily happen above  
216 a larger territory in the Carpathian Basin (Németh and Salma, 2014) as a spatially coherent  
217 regional atmospheric phenomenon (Salma et al., 2016b). Local urban NPF events are  
218 superimposed on regional events in several occasions, which result in growth curves with  
219 multiple or broad onsets. In these cases, the regional events were included in the evaluations.

220 The connection between the two sites is also one of the main reasons why the data for the city  
221 centre were complemented by the near-city background observations. Furthermore, the  
222 differences and similarities between the two locations for  $f_{\text{NPF}}$  and environmental variables  
223 (including the vegetation-related properties) could be relevant and of interest in assessing the  
224 importance of various urban environmental types in the process.

225

226 Considering that NPF events in the Carpathian Basin ordinarily extend over larger horizontal  
227 scales, long-term concentrations of NH<sub>3</sub>, which are available for the K-puszta measurement  
228 station, were also accepted in the study. This station (N 46° 57' 56", E 19° 32' 42", 125 m  
229 a.m.s.l.) is situated on the Great Hungarian Plain in a distance of 68 km from the BpART  
230 Laboratory, and it is part of the European monitoring and evaluation of the long-range  
231 transmission of air pollutants (EMEP) network. The NH<sub>3</sub> concentrations were measured in  
232 daily air samples collected by filter pack method on citric acid-impregnated cellulose filter by  
233 UV-Vis spectrophotometry according to the EMEP protocol (EMEP Manual, 2002; Horváth et  
234 al., 2009).

235

236 Most meteorological measurements for the city centre took place on site at a regular station of  
237 the Hungarian Meteorological Service (HMS, station no. 12843) in approximately 70 m from  
238 the BpART Laboratory. The data of  $T$ , RH, WS and  $P$  were obtained by standardised  
239 meteorological methods (Vaisala HMP45D temperature and humidity probe, Vaisala

240 WAV15A anemometer and Vaisala PTB210 digital barometer, respectively, all Finland) with  
241 a time resolution of 10 min (except for Y1, when it was 1 h). The WS was measured above the  
242 rooftop level. The basic meteorological data for the near-city background were derived by a  
243 mobile meteorological station installed at the measurement location at a height of ca. 2 m from  
244 the ground with a time resolution of 10 min. Global solar radiation was measured by the HMS  
245 (station no. 44527; CMP11 pyranometer, Kipp and Zonen, The Netherlands) situated in 10 km  
246 in E direction with a time resolution of 1 h. Since 2018, the GRad has been also measured on  
247 site by the BpART Laboratory on the rooftop of the building complex using an SMP3  
248 pyranometer (Kipp and Zonen, The Netherlands) with a time resolution of 1 min. The annual  
249 mean GRad ratio and SD for 1-h mean values at the BpART Laboratory and HMS station in  
250 2018 were  $1.03 \pm 0.23$  for  $\text{GRad} > 100 \text{ W m}^{-2}$ .

251

252 The Open Database for Climate Change Related Impact Studies in Central Europe (FORESEE,  
253 v. 3.1; Dobor et al., 2014) was utilized to estimate the daily maximum  $T$  data for vegetated  
254 territories within the modelled area (Fig. 1) to study the effect of  $T$  on biogenic emissions. The  
255 updated data base (<http://nimbus.elte.hu/FORESEE/>) contains observation-based spatially  
256 interpolated daily meteorological fields on a regular grid with a spatial resolution of  $1/6^\circ \times 1/6^\circ$   
257 for the interval of 1951–2019 using the E-OBS 17e dataset (Cornes et al., 2018). From the daily  
258  $T$  data 8-day means were calculated at the pixel level on the finer grid of the MODIS products  
259 using elevation as supplementary data (Kern et al., 2016). From these  $T$  data, area mean values  
260 were calculated for those pixels which represent vegetated territories (Sect. 2.2.2). Finally, the  
261 difference of the daily maximum  $T$  values from its related multi-annual mean in its  
262 corresponding 8-day time interval were determined as anomaly in maximum air temperature.  
263 In order to assist the later comparison of this differential effect with that of other environmental  
264 properties, the  $T$  anomaly was divided by the SD of the overall mean maximum air temperature  
265 (thus, it was expressed in units of SD). The quantity is referred as standardised  $T$  anomaly.  
266 Standardised NPF occurrence frequency anomaly –used in Sect. 3.3 – was calculated in an  
267 analogous manner to  $T$ .

## 268 **2.2 Modelled data**

269 Condensation sink for vapour molecules (represented by  $\text{H}_2\text{SO}_4$ ) onto the surface of existing  
270 aerosol particles was computed for discrete size distributions (Kulmala et al., 2013; Dal Maso  
271 et al., 2002, 2005) by computation scripts developed at the University of Helsinki. Dry particle  
272 diameters were considered in the calculations. One of the key components in NPF process is



273 the gas-phase H<sub>2</sub>SO<sub>4</sub> (Sihto et al., 2006; Sipilä et al., 2010; Erupe et al., 2011; Lehtipalo et al.,  
274 2018). Its long-term atmospheric measurements are demanding and, therefore, rare. The H<sub>2</sub>SO<sub>4</sub>  
275 concentrations were determined utilising a recently improved method of Dada et al. (2020)  
276 which also involves the dimer formation, by adopting the fitted coefficients for Budapest and  
277 for radiation intensities >50 W m<sup>-2</sup>. The [H<sub>2</sub>SO<sub>4</sub>] data obtained were also compared to its proxy  
278 derived as [SO<sub>2</sub>]×GRad/CS (Petäjä et al. 2009), which was used previously for many years.  
279 The calculations were based on direct on-site H<sub>2</sub>SO<sub>4</sub> measurements performed by chemical  
280 ionization atmospheric-pressure interface time-of-flight (CI-APi-TOF) mass spectrometry  
281 (Jokinen et al., 2012) in March-April 2018. Their results were utilied to derive dedicated fitting  
282 parameters for Budapest for radiation intensities >50 W m<sup>-2</sup>. The H<sub>2</sub>SO<sub>4</sub> concentrations were  
283 calculated in a retrospective manner for the other years or intervals as well. The overall data  
284 set was also compared to the proxy values derived as [SO<sub>2</sub>]×GRad/CS (Petäjä et al., 2009),  
285 which were used in our earlier studies for many years. There was a reasonable agreement in  
286 the relative changes of the two different data sets, e.g. the overall Pearson's coefficient of  
287 correlation was R=0.85. A rigorous evaluation has been finished and is to be presented in a  
288 future article.

## 289 **2.2.1 Vegetation properties related to emissions**

290 Terrestrial ecosystems emit large amounts of biogenic VOCs (BVOCs) into the atmosphere  
291 (Guenther et al., 2012). Of them, monoterpenes were identified as major aerosol precursors,  
292 and their low-volatility oxidation products were shown to play a role in NPF events (Kulmala  
293 et al., 2013; Ehn et al., 2014). Their relative importance, for instance, in the growth process  
294 increases with particle size (Riipinen et al., 2011). The requested vapour supersaturations are  
295 maintained by fast gas-phase auto-oxidation of VOCs (Crouse et al., 2013). Atmospheric  
296 concentrations of the monoterpenes can be determined online by proton transfer reaction mass  
297 spectrometry (Taipale et al., 2008), while their oxidation products can be measured by CI-APi-  
298 TOF mass spectrometry (Jokinen et al., 2015). These data are, however, usually available for  
299 shorter time intervals only. As a consequence, concentrations of both the monoterpenes and  
300 their oxidation products are estimated by proxies (Kontkanen et al., 2016). The models take  
301 into account temperature-controlled emissions from vegetation, dilution caused by mixing  
302 within the planetary boundary layer and different oxidation processes (Kontkanen et al., 2016;  
303 Lehtipalo et al., 2018). The models are available and advised for forest ecosystems.

304

305 In the present study, we derived three compound vegetation properties, i.e. GPP, LAI and SCT  
306 to evaluate the impact of BVOC sources on NPF event occurrence in urban environments.  
307 These three parameters ~~may be can~~ indirectly also be associated with vegetation emissions and  
308 finally with BVOC concentrations (Hidy et al., 2016). They were computed by the Biome-  
309 BGCMuSo biogeochemical model (v6; Thornton and Rosenbloom, 2005; Hidy et al., 2016).  
310 This is a widely used, process-based model with multilayer soil module that simulates the  
311 storage and flux of H<sub>2</sub>O, C and N between terrestrial managed agro-ecosystems and the  
312 atmosphere. The system is driven by daily meteorological data, eco-physiological properties,  
313 soil parameters and some optional input data such as CO<sub>2</sub> concentration and some site-specific  
314 management information to simulate the biogeochemical processes of a biome. It also accounts  
315 for fertilization, harvest and crop rotation. The system utilised here was parameterized  
316 specifically to the Carpathian Basin, and its proper functioning and outputs were validated by  
317 agricultural-related data products and eddy-covariance measurements (Barcza et al., 2010;  
318 Hidy et al., 2016).

319

320 Primary production of the vegetation on land depends on many factors, principally on local  
321 hydrology, soil fertility, plant species composition, photosynthetically active radiation and  
322 disturbance. It is often thought to be proportional to general biogenic activity which involves  
323 BVOC emissions as well. In Biome-BGCMuSo the GPP was calculated using Farquhar's  
324 photosynthesis routine (Farquhar et al., 1980). The LAI is a measure for the total area of leaves  
325 per unit ground area and is directly related to the amount of light that is intercepted by plants.  
326 Virtually, it is considered as a driving parameter for biosphere-atmosphere exchange of CO<sub>2</sub>  
327 and water vapour (Bonan, 2015). The SCT is a measure of the transport rate of H<sub>2</sub>O vapour  
328 exiting through the stomata of leaves, and it also controls parallel assimilation of CO<sub>2</sub>. It is a  
329 function of the density, aperture and size of stomata, and is also related to the boundary layer  
330 resistance of the leaf and the concentration gradient of H<sub>2</sub>O vapour between the leaf and the  
331 atmosphere. Light is the primary stimulus engaged in this process, the second key factor is the  
332 photosynthesis, while plants themselves can also regulate their transpiration rate via their SCT.  
333 Other (organic) gases from plants are also emitted through stomata, and, therefore, the SCT  
334 can also be related to the fluxes of BVOCs from vegetation to the atmosphere. The three  
335 vegetation-related variables were derived in model calculations for a circular geographical area  
336 around Budapest with a radius of 100 km (Fig. 1). Biome-BGCMuSo was run with generic  
337 maize, winter wheat, grassland and broadleaf forest parameterization representing the main

338 plant functional types (PFT) in the region. The model results were aggregated according to the  
339 share of PFT within the given pixel area.

### 340 2.2.2 Vegetation growth dynamics

341 Two phenological indices which are related to vegetation growth dynamics in springtime were  
342 estimated. They are the SoS, which is the onset of vegetation growth after the winter dormancy  
343 and the GuD, which expresses the time period of initial leaf development after SoS. Their  
344 determination was accomplished by utilizing the satellite-based Normalized Difference  
345 Vegetation Index (NDVI) data sets. The NDVI is a widely used remote-sensing-based measure  
346 of the terrestrial vegetation greenness and state, defined as

$$347 \text{NDVI} = \frac{R_{\text{NIR}} - R_{\text{Red}}}{R_{\text{NIR}} + R_{\text{Red}}}, \quad (1)$$

349 where  $R_{\text{NIR}}$  and  $R_{\text{Red}}$  are the surface reflectances acquired in the near-infrared (NIR,  $\lambda=700\text{--}$   
350 1100 nm) and red regions of the spectra, respectively (Rouse et al., 1974). The pigment in live  
351 green leaves (chlorophyll) strongly absorbs light in the photosynthetically active range of 400–  
352 700 nm (for use in photosynthesis), while its cell structure strongly reflects or reemits radiation  
353 in the NIR region (and green light) compared to other wavelengths. The NDVI is, therefore,  
354 directly related to the photosynthetic capacity of plant canopies. They were actually derived  
355 from the latest version (C006) of the official MOD09A1 atmospherically corrected surface  
356 reflectance product (Vermote, 2015). This was generated from the measurements of the  
357 MODerate resolution Imaging Spectroradiometer (MODIS) operating on board of the satellite  
358 EOS AM1, Terra (Justice et al., 1998). The data were downloaded for the h19v04 sinusoidal  
359 tile with a spatial resolution of 500 m and a temporal resolution of 8 d (LP DAAC, 2019) in  
360 hierarchical data format for the interval of 2009–2019.

361  
362  
363 The land cover data sets for a circular area with a radius of 100 km around Budapest were  
364 derived from the official MCD12Q1 land cover product (Sulla-Menashe and Friedl, 2018) with  
365 a spatial resolution of 500 m for years 2001–2018 according to the International Geosphere  
366 Biosphere Programme (IGBP) classification scheme (Fig. 1). In the modelling, the following  
367 vegetation types were studied: 1) croplands (58 % of all, 117817 pixels), 2) grasslands (13 %),  
368 3) deciduous broadleaf, mixed and evergreen needleleaf forests (12 %; of them, 98 % deciduous

369 trees) and 4) all vegetation, i.e. all territory types except for urban and built-up lands (6 %),  
370 water bodies (0.9 %) and permanent wetlands (0.6 %).

371

372 Daily-resolution data set was calculated after quality filtering and pre-processing, and then the  
373 characteristics of the spring development were assessed by the methodology of Kern et al.  
374 (2020). From remote-sensing point of view, the green-up dynamics is characterized by a sharp,  
375 mostly linear rise in the NDVI curve that represents leaf flushing (Seyednasrollah et al., 2018),  
376 and which can be characterized by the date of leaf unfolding (as the SoS). The GuD is the time  
377 difference between the date of the end of greening (EoG) and of the SoS. To achieve this, the  
378 NDVI span was calculated as the difference between the maximum and the minimum NDVI  
379 during spring green-up. The SoS and the EoG were set at the date (day of year) when NDVI  
380 reached the lower and upper 20 % of the NDVI span, respectively (e.g. Shen et al., 2015). The  
381 applied cut-off method is commonly used to determine the start of the season of a biome. Both  
382 the SoS and GuD data were determined at the pixel level for each year. Their SDs were  
383 calculated for a given land cover type as characteristics of the spatial variability of the derived  
384 metrics. Taking into account that pixels of relatively coarse (500 × 500 m) spatial resolution  
385 can be divers in vegetation type and species with variable phenological properties, and that the  
386 processed remote sensing data are affected by noise due mainly to atmospheric, illumination  
387 or observation conditions, the derived metrics are subject to relatively large variability (cf. Fig.  
388 7). The vegetation growth for all years and the methodological procedure are summarized in  
389 Fig. S1 in the Supplement. The data sets were processed using the Interactive Data Language  
390 (v. 8.6, Harris Geospatial Solutions, USA).

### 391 **3 Results and discussion**

392 Annual averages of the environmental variables over most measurement years were already  
393 summarized in accompanying publications (Salma and Németh, 2019; Mikkonen et al., 2020),  
394 and, therefore, the new quantities studied are only overviewed in Table 1. The data are in line  
395 with or comparable to the values ordinarily obtained for the area (Barcza et al., 2010; Salma et  
396 al., 2016b).

397

398 During the seven measurement years, the total number of NPF events was 514. The annual  
399 means of the relative NPF event occurrence frequency are considerable. The overall six-year  
400 mean and SD for the city centre were (21±5) %. The  $f_{\text{NPF}}$  in year 2015–2016 was unusually low

401 (its value was ca. 13 %, thus lower by 35 % relatively than the overall mean), but there is no  
 402 plausible explanation for this extreme in the present annual data set. The overall mean  
 403 frequency and its SD imply that the annual  $f_{\text{NPF}}$  did not change substantially and, more  
 404 importantly, in a tendentious manner over the decennial interval studied. It is added as  
 405 background information that ~~1)~~ there was ~~also~~ no significant decreasing trend in major  
 406 precursors or interacting gaseous chemical species such as SO<sub>2</sub> or NO<sub>2</sub> in the area over the time  
 407 interval of interest (Mikkonen et al., 2020, see also Figs. S2 and S6, respectively). ~~and~~  
 408 2) Furthermore, the overall annual median formation rate of particles with a diameter of 6 nm  
 409 was 4.6 cm<sup>-3</sup> s<sup>-1</sup>, the median growth rate for 10-nm particles was 7.3 nm h<sup>-1</sup> over the years  
 410 studied, and they were without larger fluctuations and both showed summer maximum (Salma  
 411 and Németh, 2019).

412

413 **Table 1.** Number of NPF event days ( $n_{\text{NPF}}$ ), annual median gas-phase H<sub>2</sub>SO<sub>4</sub> concentration and NH<sub>3</sub> mixing ratio,  
 414 gross primary production (GPP) of vegetation, leaf area index (LAI) and stomatal conductance (SCT) for the  
 415 seven measurement years. The measurement units are indicated in brackets.

416

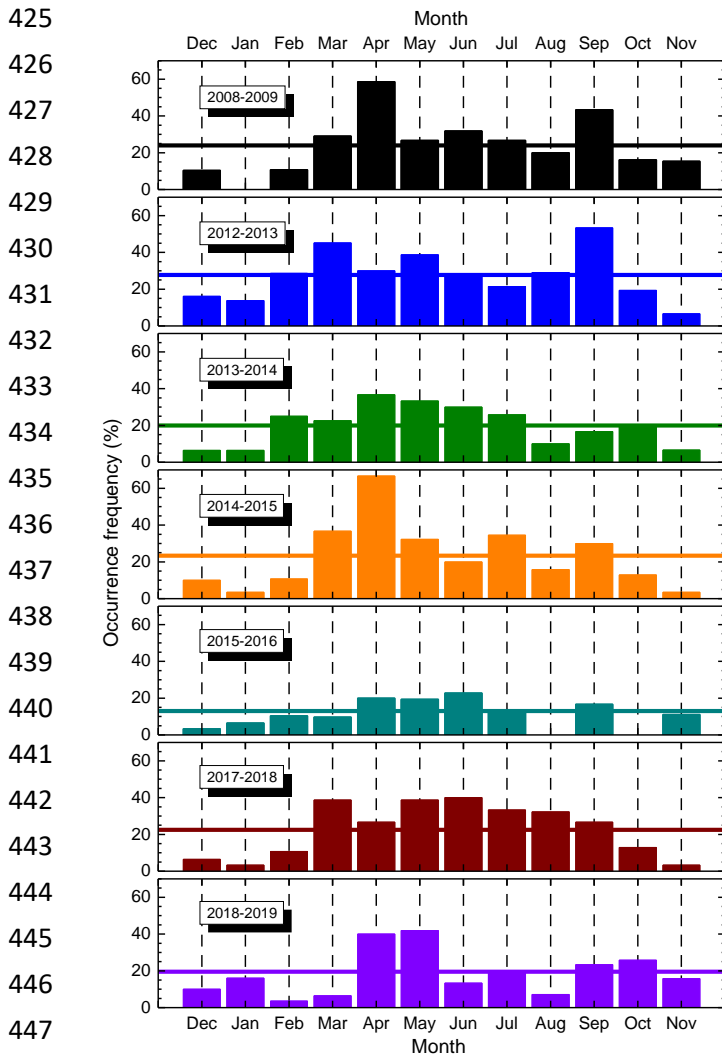
Measurement year/ Variable	2008– 2009	2012– 2013	2013– 2014	2014– 2015	2015– 2016	2017– 2018	2018– 2019
$n_{\text{NPF}}$	83	96	72	81	35	83	64
[H <sub>2</sub> SO <sub>4</sub> ] ( $\times 10^5$ cm <sup>-3</sup> )	8.8	14.5	8.4	8.7	11.5	10.0	10.4
[NH <sub>3</sub> ] (ppb)	2.1	2.0	2.8	2.3	2.5	2.6	3.1
GPP (gC m <sup>-2</sup> d <sup>-1</sup> )	2.5	2.6	3.0	2.7	3.1	2.8	2.9
LAI (%)	71	73	81	82	86	93	70
SCT ( $\times 10^{-3}$ m s <sup>-1</sup> )	1.68	1.62	2.1	1.73	2.1	1.90	1.75

417

### 418 3.1 Distributions of NPF event occurrence

419 Distributions of the monthly mean occurrence frequency of event days for each measurement  
 420 year are shown in Fig. 2. There are obvious similarities and differences among the distributions.  
 421 The largest diversity was realised in the measurement year 2015–2016 (that also exhibited the  
 422 smallest annual mean  $f_{\text{NPF}}$ ). Its shape was flattened and featureless. All the other distributions  
 423 were much closer to each other in many respects.

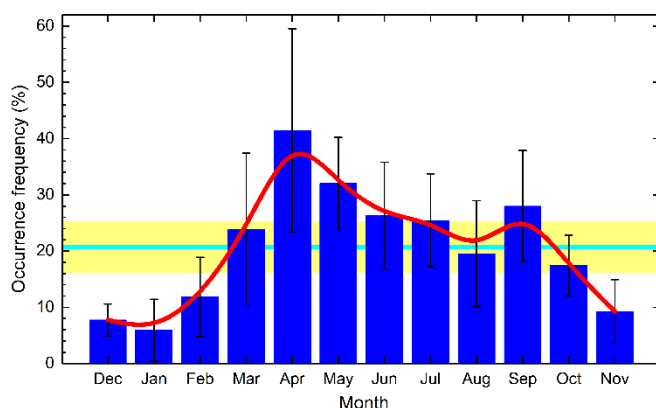
424



448 **Figure 2.** Distributions of monthly mean relative occurrence frequency of NPF event days for the seven  
 449 measurement years. The horizontal lines indicate annual means. The value for January 2009 is zero, while the  
 450 values for August and October 2016 are not available. The measurements in 2012–2013 were performed in the  
 451 near-city background, while in the other years, they were accomplished in the city centre.

452  
 453 The shapes of the individual distributions also intimated some resemblant components that  
 454 were repeated over the years. They became more obvious when the overall mean distribution  
 455 was derived by averaging for all years in the city centre (Fig. 3). The overall distribution  
 456 exhibits an evident structure which consists of an absolute and a local maximum in April with  
 457 a monthly mean occurrence frequency of  $(41 \pm 18)$  % and in September with a mean of  
 458  $(28 \pm 10)$  %, respectively and an absolute and a local minimum in January with a mean of  
 459  $(5.9 \pm 5.5)$  % and in August with a mean of  $(19.5 \pm 9.4)$  %, respectively. The relatively large  
 460 uncertainty intervals of the monthly mean frequencies were caused by inter-annual variability  
 461 (Fig. 2), and they are also influenced by the absolute number of NPF event days in separate  
 462 months, which is substantially smaller in winter months than in the other months.

463  
464  
465  
466  
467  
468  
469  
470  
471  
472



473 **Figure 3.** Mean distribution of the monthly mean relative occurrence frequency of NPF event days for the joint  
474 six-year-long data set in the city centre. The error bars show  $\pm 1$  SD, the horizontal line in cyan indicates the overall  
475 mean and the yellow band represents its  $\pm 1$  SD. The smooth curve in red serves to guide the eye.

476

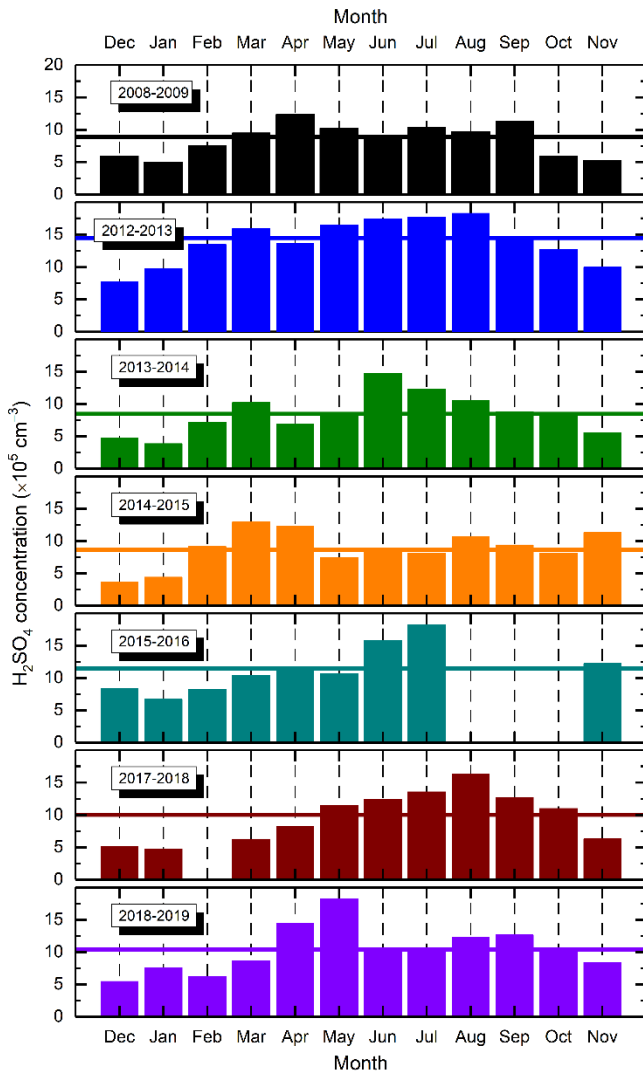
477 It seems that the overall mean distribution does not change further extensively if another new  
478 year (for example Y8) is added into the data set. This is also the reason why Fig. 3 and a related  
479 plot which was presented earlier (Fig. 1 in Salma and Németh, 2019) are similar. This all  
480 implies that the shape of the overall distribution can already be considered to be representative.  
481 Moreover, it appears to be characteristic and remarkable. Furthermore, it closely agrees with a  
482 multi-year general shape even for some very diverse and detached environments such as boreal  
483 forest (Nieminen et al., 2014). It seems, therefore, to be sensible to study the factors that lead  
484 to this general structure. We chose to display the up-to-date overall distribution here to foster  
485 its comparison to that of environmental variables within the present article.

### 486 3.2 Distributions of environmental variables

487 Distributions of the monthly mean values for environmental variables for the seven  
488 measurement years were derived. The plots for  $\text{H}_2\text{SO}_4$  concentration are shown in Fig. 4 as  
489 example. The distributions for some other selected variables, i.e. of  $\text{SO}_2$ ,  $\text{GRad}_{\text{max}}$ , CS,  $\text{O}_3$ ,  
490  $\text{NO}_2$ ,  $\text{NH}_3$ , RH, WS and  $T$  are presented in Figs. S2–S10, respectively. The monthly averages  
491 which are missing in these figures were not available.

492

493  
494  
495  
496  
497  
498  
499  
500  
501  
502  
503  
504  
505  
506  
507  
508  
509  
510  
511  
512  
513  
514  
515



516  
517  
518  
519  
520  
521  
522  
523  
524  
525  
526  
527  
528  
529  
530

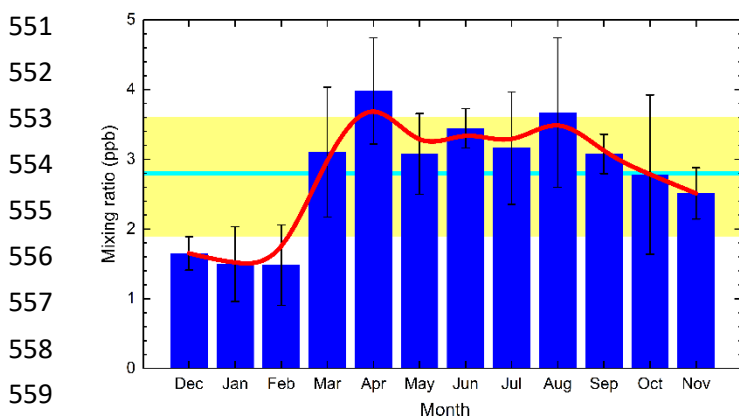
**Figure 4.** Distribution of monthly median gas-phase  $\text{H}_2\text{SO}_4$  concentration for the seven measurement years. The values for August–October 2016 and February 2018 are not available. The horizontal lines indicate annual medians. The measurements in 2012–2013 were performed in the near-city background, while in the other years, they were accomplished in the city centre.

By comparing Figs. 4 and 2, we can conclude that there are similar overall tendencies in their shape for several years. The concentration of  $\text{H}_2\text{SO}_4$  also tended to have a maximum in spring and another one in August or September. Its seasonal variation could jointly be affected mainly by  $[\text{SO}_2]$ , CS and GRad (Petäjä et al. 2009). Concentration of  $\text{SO}_2$  showed a maximum in winter (Fig. S2),  $\text{GRad}_{\text{max}}$  had a broad and obvious maximum in summer (Fig. S3), while CS tended to exhibit minimum values in summer (Fig. S4). It seems that in the first approximation, the  $f_{\text{NPF}}$  distribution is linked to the temporal cycling of  $\text{H}_2\text{SO}_4$  concentration. It does not explain, however, the temporal variability alone and other environmental variables have to play important roles in NPF occurrence.



531 For most of the other environmental properties, their connections with occurrence frequency  
 532 were even weaker or featureless (than for  $[H_2SO_4]$  and  $f_{NPF}$  pair) with some similar tendencies  
 533 reached in sporadic years. The only exception seemed to be  $NH_3$  concentration (Fig. S7). Its  
 534 overall mean distribution was derived by averaging the data for the corresponding years, and  
 535 it is shown in Fig. 5. The shape of the resulting distribution resembles the form and structure  
 536 of the overall  $f_{NPF}$  distribution (cf. Fig. 3). It also contains an absolute maximum in April and  
 537 an absolute minimum in January-February, and perhaps a local maximum in August. The  
 538 situation is, however, complicated by the dissociation equilibrium in  $NH_4NO_3$  (solid or liquid),  
 539  $NH_3$  (gas) and  $HNO_3$  (gas) thermodynamic system, which is rather sensitive to  $T$ ,  $RH$  and  
 540 particle size or solution concentration and  $pH$  (Mozurkewich, 1993; Nenes et al., 2020).  
 541 Ambient gas-phase  $[NH_3]$  are regulated and modified by this equilibrium as well. The  
 542 similarities in the shapes and the coincidence in the extremes for the two variables may suggest  
 543 that the availability of  $NH_3$  gas – as a base chemical compound in the atmosphere – can enhance  
 544 the nucleation of  $H_2SO_4$  molecules in the ambient air thus, NPF event occurrence. This is in  
 545 line with results from chamber experiments (Kirkby et al., 2011), while the involvement of  
 546  $NH_3$  in NPF under relatively warm ambient conditions (close to the land surface in the  
 547 atmosphere) has not been completely clarified yet (Kürten, 2019). It also raises a question  
 548 whether other relevant atmospheric chemical bases such as amines have in general or in  
 549 synergy with  $NH_3$  a similar role in the area.

550



551  
 552  
 553  
 554  
 555  
 556  
 557  
 558  
 559  
 560 **Figure 5.** Mean distribution of the monthly mean  $NH_3$  mixing ratio for the joint six-year-long data set in the city  
 561 centre. The error bars show  $\pm 1$  SD, the horizontal line in cyan indicates the overall mean and the yellow band  
 562 represents its  $\pm 1$  SD. The smooth curve in red serves to guide the eye.

563

564 Pearson's coefficients of correlation between  $f_{NPF}$  and the other variables in the joint monthly  
 565 mean data set were typically  $|R| < 0.50$ , except for  $RH$ ,  $G_{Rad_{max}}$ ,  $NO$ ,  $O_3$  and  $NH_3$ , which were

566 –0.72, 0.70, –0.61, 0.58 and 0.53, respectively. It is added that the variables influence the  
567 occurrence jointly, and, therefore, the pair wise correlation may not be fully satisfactory for  
568 revealing their relationships. These particular results (and the mean event-day-to-non-event-  
569 day ratios in Sect. 3.4) prepare further comprehensive multi-statistical analyses.

570

571 Another possible explanation of the characteristic structure could be related to the idea that  
572 NPF events often occur in elevated heights (as they are favoured at lower  $T$ s) and the nucleated  
573 particles are mixed down toward the land surface by general effects of turbulent mixing and  
574 air temperature which can have annual cycling. Dedicated measurements on this issue have  
575 been in progress to clarify this proposal (Carnerero et al., 2018).

### 576 **3.3 Temperature anomaly**

577 Possible impacts of  $T$  on NPF occurrence exerted indirectly through vegetation was further  
578 investigated by using anomalies. The anomaly emphasises the deviation of an environmental  
579 property (for a given time interval, here for a month or week) from its multi-year trend. The  
580 standardised anomaly is expressed in units of SD of the whole data set considered. The  
581 anomalies in maximum  $T$  and in NPF occurrence frequency were determined as described in  
582 Sec. 2.1, with SDs of 3.1 °C and 13 %, respectively. Their time distributions (Fig. 6) resembled  
583 fluctuations as expected.

584

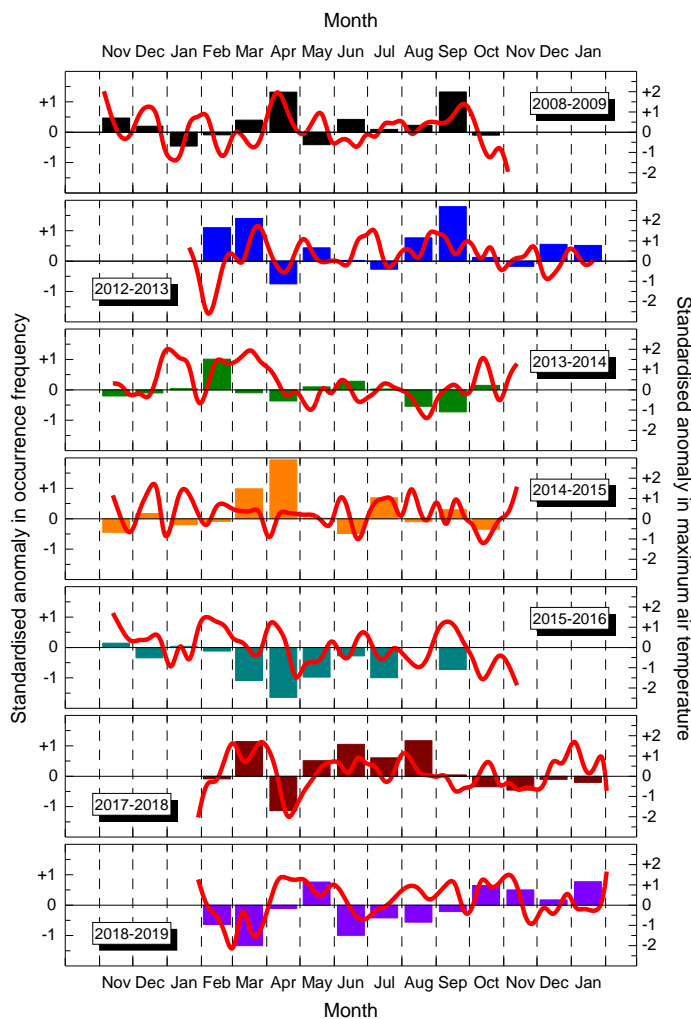
585 First, the possible impacts of standardised anomaly in maximum  $T$  above vegetated territories  
586 on the extreme values of monthly NPF occurrence frequency was examined. This can be  
587 achieved by comparing the column plots in Fig. 2 with the  $T$  anomaly lines in Fig. 6 for each  
588 year. (Their joint graph is shown in Fig. S11.) In many cases (e.g. in spring 2008, 2012, 2017  
589 and 2018), the absolute (spring) maximum of the occurrence frequency overlapped with or  
590 followed a substantial positive  $T$  anomaly. The exceptions were the years 2014–2015 (Y4) and  
591 2015–2016 (Y5). This suggests that NPF events are generally favoured or possibly are linked  
592 to larger  $T$ s in spring. The impact of  $T$  is, however, part of more comprehensive environmental  
593 interactions. No similar observation could be made with respect to the absolute minimum  $f_{\text{NPF}}$ .  
594 This implies that the lowest NPF occurrence in winter is most likely not restricted by  $T$ .

595

596 The effect of the potential heat stress exerted on plants in sultry summer intervals has become  
597 a relevant issue in the Carpathian Basin because of climate change. During these extremely  
598 warm intervals, the plants could emit less VOCs since their stomata are more closed to reduce

599 the rate of transpiration (Sect. 2.2.1). The coincidence between the positive  $T$  anomaly and  
 600 summer minimum  $f_{NPF}$  could not be, however, established in the present data set.

601  
 602  
 603  
 604  
 605  
 606  
 607  
 608  
 609  
 610  
 611  
 612  
 613  
 614  
 615  
 616  
 617  
 618  
 619  
 620  
 621  
 622  
 623



624 **Figure 6.** Time distribution of anomalies standardised to annual SD of the variable in maximum air temperature  
 625 above vegetated territories (red lines) and in monthly mean NPF occurrence frequency (column charts) for the  
 626 seven measurement years.

627

628 As the next step, the variability of the standardised anomaly in maximum  $T$  above vegetated  
 629 territories and in monthly NPF occurrence frequency were investigated (Fig. 6) to assess the  
 630 sensitivity of NPF to  $T$ . Some temporal tendencies between the two anomalies change in line  
 631 although their variability seems loose or not coherent in some other intervals. This can partially  
 632 be explained by multi-factorial impacts of environmental variables including vegetation-  
 633 derived quantities. There could also be some delay in the relationship between  $T$  and  $f_{NPF}$ . It  
 634 emphasizes again the need for multi-variate statistical evaluation methods comprising cross-  
 635 connections among the variables, which is going to be part of a next dedicated study.

636

637 In addition, the monthly or 8-d mean values evaluated so far do not necessarily capture the  
638 potential relationships among the variables fully since they may take effect on shorter, e.g.  
639 daily time scale, which could be of not less importance from the point of NPF view. In order  
640 to extend our study to shorter time intervals, we continued investigating the daily mean data.

### 641 **3.4 Event-day-to-non-event-day ratios**

642 The monthly and annual mean ratios of ~~the-all~~ environmental variables observed on NPF event  
643 day and on non-event days in the city centre are summarised in Table 2. The relative occurrence  
644 frequencies of event days were also given for comparative purposes. The ratios can be  
645 influenced again by the number of event days. The uncertainty of the ratios for ~~the~~-modelled  
646 variable could be as high as 30 % or even larger if the monthly mean data are relatively small  
647 (e.g. for GPP, LAI and SCT in winter). The variables with annual ratios of approximately  
648  $r_{an}>1.1$  can be considered to favour or to be associated with NPF occurrence in general, the  
649 variables with approximately  $r_{an}<0.9$  can be regarded to disfavouring events, while the  
650 variables with  $r_{an}$  between these two limits possibly have low influence on NPF. The specified  
651 values serve only as indicative or guide ratios. The criteria were selected so that the variability  
652 of the daily mean values around the monthly mean ordinarily remains between them. This was  
653 based upon a simple exercise with non-event time intervals. The procedure represents a  
654 pragmatic approach, though alternative limits could also be set.

655

656 It is the H<sub>2</sub>SO<sub>4</sub> that shows the largest annual mean ratio. The atmospheric concentration of  
657 H<sub>2</sub>SO<sub>4</sub> was larger by a factor of ca. 1.5 on event days than on non-event day. The ratio was  
658 even larger in winter months (a mean factor of 1.8) over which the other chemical and  
659 meteorological conditions for NPF are less favourable than in general. In winter, NPF events  
660 happen if H<sub>2</sub>SO<sub>4</sub> is available in relatively large excess concentrations ~~which can ensure the~~  
661 ~~required supersaturation~~. For all the other months, the mean ratios were also larger than unity.  
662 The smallest monthly mean ratio was obtained in July (and possibly in August and September).  
663 This all confirms the primary role of H<sub>2</sub>SO<sub>4</sub> in the phenomenon.

664

665 The second largest annual mean ratio was found for O<sub>3</sub>. Its larger concentrations are often  
666 associated with general photochemical activity and secondary organic aerosol (SOA) formation  
667 (McFiggans et al., 2019). Its influence ~~—was also~~ represented by the ratio of the monthly mean  
668 event-day-to-non-event-day ratio to its annual mean ratio. ~~—in winter~~ The ratio of ratios for O<sub>3</sub>

669 in winter was the largest (1.64) of all ~~relative-ratios~~cases. This all implies that the  
670 photochemical reactivity, involving e.g. the H<sub>2</sub>SO<sub>4</sub> formation in the gas phase and the VOC  
671 oxidation, also plays an important role particularly in those months when the absolute oxidative  
672 property is relatively low (Fig. S5 for O<sub>3</sub>).

673

674 **Table 2.** Overall mean relative occurrence frequency of NPF event days ( $f_{\text{NPF}}$  in percent) and overall mean event-  
675 day-to-non-event-day ratios for daily median concentration of gas-phase H<sub>2</sub>SO<sub>4</sub> and O<sub>3</sub>, daily maximum GRad  
676 (GRad<sub>max</sub>),  $N_{6-100}$ ,  $N$ , WS, gross primary production (GPP) of vegetation, stomatal conductance (SCT), SO<sub>2</sub>, leaf  
677 area index (LAI), NO<sub>2</sub>,  $P$ , NO, NH<sub>3</sub>, PM<sub>10</sub> mass, CO, CS,  $N_{100-1000}$  and RH for each month and for all data in the  
678 city centre. The ratios were organised in descending order of their annual mean values (the first data column).

679

Interval/ Variable	Annual	Dec	Jan	Feb	Mar	Apr	May	Jun	Jul	Aug	Sep	Oct	Nov
$f_{\text{NPF}}$	21	7.8	5.9	11.8	24	41	32	26	25	17.0	26	17.4	9.3
H <sub>2</sub> SO <sub>4</sub>	1.54	1.61	2.2	1.66	1.38	1.40	1.35	1.40	1.19	1.29	1.29	1.59	1.56
O <sub>3</sub>	1.42	2.6	2.6	1.79	1.20	0.99	1.09	1.18	0.97	1.07	0.99	1.26	1.28
GRad <sub>max</sub>	1.32	1.71	1.56	1.47	1.24	1.26	1.19	1.12	1.05	1.17	1.13	1.44	1.48
$N_{6-100}$	1.25	1.06	0.88	1.18	1.11	1.60	1.46	1.13	1.21	1.52	1.38	1.20	1.28
$N$	1.17	0.92	0.78	1.08	1.05	1.52	1.40	1.10	1.15	1.44	1.31	1.10	1.19
WS	1.16	1.68	1.66	1.23	1.18	0.92	0.97	1.14	1.15	0.77	0.97	1.21	1.00
GPP	1.14	1.47	0.99	1.06	1.20	1.20	1.12	0.98	1.06	1.06	0.97	0.90	1.72
SCT	1.10	1.22	1.11	0.98	1.17	1.08	0.97	0.95	1.16	1.01	1.04	0.90	1.61
SO <sub>2</sub>	1.08	0.88	0.82	1.01	1.05	1.20	1.18	1.18	1.09	1.22	1.11	1.05	1.20
LAI	1.05	0.98	1.02	1.01	1.16	1.05	1.01	0.97	1.04	0.98	0.99	0.82	1.54
NO <sub>2</sub>	1.02	0.93	0.86	1.00	0.86	1.15	1.18	0.95	0.89	1.13	1.09	1.05	1.09
$P$	1.00	1.00	1.00	1.00	1.00	1.00	1.00	1.00	1.00	1.00	1.00	1.00	1.00
NO	0.99	0.65	0.52	0.80	0.95	1.25	1.37	0.88	0.92	1.03	1.18	1.07	1.19
NH <sub>3</sub>	0.96	0.90	0.91	0.88	0.82	1.04	1.12	1.03	0.86	0.86	1.03	1.14	0.93
PM <sub>10</sub>	0.95	0.71	0.71	0.87	0.81	1.08	1.16	1.05	0.99	1.01	1.08	0.94	1.02
CO	0.94	0.78	0.69	0.88	0.89	1.06	1.03	1.01	0.90	0.95	1.08	0.90	1.10
CS	0.90	0.53	0.55	0.77	0.82	1.17	1.16	0.95	0.91	1.20	1.04	0.78	0.97
$N_{100-1000}$	0.89	0.50	0.53	0.78	0.82	1.16	1.14	0.97	0.90	1.18	1.03	0.77	0.97
RH	0.87	0.78	0.85	0.83	0.93	0.88	0.85	0.89	0.90	0.85	0.92	0.86	0.91

680

681 The GRad<sub>max</sub> exhibited the third largest annual mean ratio, and its monthly mean ratios were  
682 also above unity. This property is related to the both variables discussed above and, therefore,  
683 those arguments are valid here as well. It was shown that the presence of clouds decreases the  
684 probability of NPF occurrence by attenuating solar radiation intensity below the cloud layer  
685 (Baranizadeh et al., 2014; Dada et al., 2017), and that an ongoing event can even be interrupted  
686 by a sudden appearance of clouds (Hirsikko et al., 2013; Salma et al., 2016a).

687

688 The large annual mean ratios for  $N$  and in particular for  $N_{6-100}$  are rather consequences of NPF  
689 events than their causes. Ultrafine (UF) particles are generated by NPF and growth processes  
690 in a large number. It is worth noting that the largest ratios of 1.5–1.6 happened in April, May  
691 and August, while the smallest ratio, which was below unity (0.88), was realised in January.  
692 This can partially be linked to the monthly variation of the particle formation and growth rates  
693 in Budapest as well (Salma and Németh, 2019). The interpretations of these ratios are in line  
694 with our earlier assessments or findings according to which 1) the concentrations of particles  
695 are increased by a factor of 2–3 on event days in central Budapest and 2) the NPF contribution  
696 as a single source of UF particles is ca. 13 % as a lower estimate and on longer run (Salma et  
697 al., 2017).

698  
699 The effect of WS seems to be also noteworthy. On annual scale, higher WSs can be related to  
700 larger event occurrences. The distribution of its monthly mean, however, reveals a more  
701 complex relationship. In the months with large relative occurrence frequency (i.e. in April,  
702 May and September), the mean ratios were below unity (0.92 in April), in the winter months,  
703 they were extensively above unity (1.52), while they were very close to unity in the other  
704 months. This behaviour will be explained later in connection with CS and  $N_{100-1000}$ .

705  
706 Precursor BVOC gases – approximated by GPP, LAI and SCT – and  $\text{SO}_2$  may generally favour  
707 NPF occurrence although their influence could not be quantified and seems to be low. The  
708 reason for this could partially be that the oxidation rates of precursors appear to be more  
709 important than their atmospheric concentrations (Salma and Németh, 2019), and that the effect  
710 of photochemical processes could be delayed in time. The concentrations of BVOCs are  
711 expected to be considerable in Budapest in spring. The typical mean contribution of biogenic  
712 sources to the total carbon in the  $\text{PM}_{2.5}$  size fraction was the second largest with a share of ca.  
713 40 % (Salma et al., 2020). Unfortunately, there is no experimental information available on  
714 absolute concentrations or amounts of VOC in the area. The effects of  $\text{NO}_2$ ,  $P$  and  $\text{NO}$  seemed  
715 to be even more constrained. Concentrations of  $\text{CO}$  and  $\text{PM}_{10}$  mass are often accounted as  
716 surrogates for urban air quality; and the polluted air seems to suppress NPF occurrence through  
717 high CS. Again, the monthly mean event-day-to-non-event-day ratios for  $\text{NO}$ ,  $\text{PM}_{10}$  mass and  
718  $\text{CO}$  were the smallest (typically 0.66, 0.76 and 0.78, respectively) in winter, when the  
719 preconditions of events are reached in a more difficult manner.

720

721 The mean ratios of CS and  $N_{100-1000}$  were close to each other and mostly below unity. Their  
722 lowest values of around 0.53 were reached in December and January. This implies that the NPF  
723 events preferably took place in winter on those days when the concentrations of pre-existing  
724 particles were relatively small. The whole issue can be explained if considering that the basic  
725 preconditions of NPF events are realised by competing sources and sinks for condensing  
726 vapours. The source strength in winter is generally low due to lower solar radiation intensities  
727 and less biogenic precursor gases in the air. New particle formation events can occur at these  
728 low source intensities if the condensation and scavenging sinks – which are related to low  
729 particle number concentrations – are even smaller (Lehtinen et al., 2007). This can happen, for  
730 instance, due to a stronger wind (Fig. S9) which brings in low concentrations of regional and  
731 chemically aged particles ( $N_{100-1000}$ ) into city centres. The reasoning above is in line with and  
732 confirms our earlier findings related to diurnal and seasonal variations of UF particles (Salma  
733 et al., 2014, 2017).

734

735 The smallest annual mean event-day-to-non-event-day ratio was obtained for RH. All monthly  
736 mean ratios were also below unity and were similar to each other with an annual mean and SD  
737 of  $0.87 \pm 0.04$  (cf. Fig. S8). This unambiguously indicates that RH counteracts to NPF  
738 occurrence. It can serve as scavenger for OH radical (Petäjä et al., 2009). The dependency was  
739 already observed in earlier studies on continental NPF processes (Hamed et al., 2011).

740

741 It is noted for completeness that the mean event day minus non-event day  $T$  difference in the  
742 city centre for various months were 1.2 (Dec), 0.4 (Jan),  $-0.8$  (Feb), 0.4 (Mar), 1.5 (Apr), 1.9  
743 (May), 0.1 (Jun),  $-0.8$  (Jul), 0.1 (Aug),  $-0.5$  (Sep), 1.8 (Oct) and 1.4 °C (Nov). (The mean  
744 event-day-to-non-event-day ratios for  $T$  in a unit of K were all 1.00.) The monthly mean air  
745 temperature data do not indicate obvious relationships with  $f_{\text{NPF}}$  (cf. also Fig. S10). This is  
746 contrasting with its effect on NPF dynamic properties, for which the  $T$  causes summer maxima  
747 (Lee et al., 2019; Salma and Németh, 2019). The latter effect can be facilitated, for instance,  
748 through gas-phase auto-oxidation reactions involved in HOMs formation (Frege et al., 2018).  
749 The monthly and annual mean ratios of  $[\text{NH}_3]/\text{CS}$ ,  $\text{GPP}/\text{CS}$ ,  $\text{LAI}/\text{CS}$  and  $\text{SCT}/\text{CS}$  on NPF event  
750 days and on non-event days in the city centre were also derived considering that  $\text{NH}_3$  and  
751 BVOCs could in principle play a driving role in the events. The monthly ratios did not exhibit  
752 tendentious variation and did not resemble the distribution of occurrence frequency (Fig. 3).  
753 This and the concentration ratios for  $\text{NH}_3$  do not explicitly support the indications on its

754 possible outstanding role (Sect. 3.2) and, therefore, further dedicated systematic studies are  
755 required in the area to arrive at conclusive overall interpretation of NH<sub>3</sub>. The plans should  
756 preferably comprise other chemical species as well such as BVOCs or anthropogenic organics.  
757 It is added that the effect of an environmental variable can depend on its absolute value as well.  
758 This can exhibit seasonal or other variability in time (Kerminen et al., 2018). The absolute  
759 values can also change from site to site and, furthermore, there can be different interactions or  
760 biases among some variables at different sites. Moreover, even dominant nucleation or growth  
761 mechanisms can vary at a fixed location depending on the availability of precursors or of  
762 different types of oxidation agents (e.g. OH, O<sub>3</sub> or NO<sub>3</sub>, Bianchi et al., 2016). These all factors  
763 can modify the effect of a variable. Strictly speaking, the interpretations above are, therefore,  
764 related to the region investigated. These aspects likely explain why the effects of some  
765 variables were interpreted inconclusively. For instance, both higher (Birmili and Wiedensohler  
766 2000; Zhao et al., 2015) and lower (Wu et al., 2007) SO<sub>2</sub> concentrations on event days relative  
767 to non-event days were reported at diverse locations.

### 768 **3.5 Vegetation growth**

769 The SoS and the GuD data are summarised in Table 3 for all vegetation. It is seen that the  
770 spring typically starts in the Budapest area around 28 March, and that the green-up of  
771 vegetation takes ordinary 40 days. These characteristics were, however, diverse when different  
772 vegetation types were considered. The SoS increased monotonically in the order of croplands,  
773 grasslands and forests. The spring started 2–3 days earlier for cultivated crops than for all  
774 vegetation, the start was almost identical for grass and all vegetation, while it was delayed by  
775 ca. 9 days for forest with respect to all vegetation. At the same time, the GuD for grasslands  
776 and croplands were identical (42–43 d), while the green-up was faster by 32 % for forests (27 d)  
777 than for all vegetation. This all can likely be explained by phyto-physiological properties of  
778 the different plants, seeding routine of cultivated crops and increasing intensity of solar  
779 radiation (and  $T$ ) in the course of springtime.

780



781 **Table 3.** Start of spring (SoS) with its SD ( $SD_{SoS}$ ) and the green-up duration (GuD) with its SD ( $SD_{GuD}$ ) for all  
 782 vegetation within a 100-km diameter circular area around Budapest for all measurement years. The years in  
 783 brackets indicate the calendar year of the spring.

784

Property	Year/ Unit	Y1 (2009)	Y2 (2012)	Y3 (2014)	Y4 (2015)	Y5 (2016)	Y6 (2017)	Y7 (2018)	Y8 (2019)	Mean
SoS	date	02 Apr	03 Apr	18 Mar	30 Mar	26 Mar	25 Mar	02 Apr	23 Mar	28 Mar
SoS	day of year	92	94	78	89	86	84	92	82	87
$SD_{SoS}$	d	12	14	17	18	17	12	15	16	–
GuD	d	33	39	42	43	42	41	32	49	40
$SD_{GuD}$	d	18	15	20	18	19	16	17	19	–

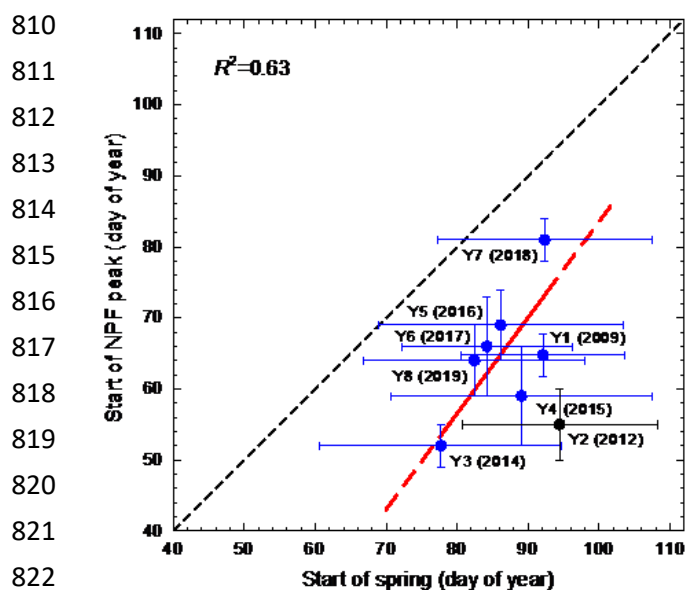
785

786 The scatter plot of the SoS date for all vegetation and the start of NPF event occurrence spring  
 787 peak is shown in Fig. 7. It is recalled that the measurements in 2012–2013 (Y2) were conducted  
 788 in a forest clearing in the near-city background (Sect. 2.1, [description of the measurement sites](#)),  
 789 and that the growth characteristics are different for various vegetation types as just concluded  
 790 [in the paragraph](#) above. For this reason, the data point for year Y2 was excluded from the  
 791 further evaluations. We kept displaying it in Fig. 7, but it is shown in a different (black) colour  
 792 from the other points to emphasize this. It is seen that the NPF spring occurrence reacted more  
 793 sensitively than the visible vegetation spring or green-up in general. This outcome agrees with  
 794 our long-term sensing perceptions. More importantly, a clear relationship between the NPF and  
 795 SoS timing could be identified. The Pearson’s coefficient of correlation of the data set was  
 796  $R=0.80$ . Their link was expressed by a linear fit utilizing weighted least-squares method. The  
 797 goodness of the fit was quantified by the coefficient of determination, which was  $R^2=0.63$ . The  
 798 statistical quantities above support that the association between vegetation dynamics and NPF  
 799 occurrence is significant. We are aware that the two properties are likely biased by other  
 800 variables such as e.g. GRad, and, therefore, the interpretation of their causal relationship or  
 801 direct links are subject to further dedicated investigations.

802

803 The relationships of GuD for all vegetation and the total number of NPF events in spring, the  
 804 maximum monthly occurrence frequency in spring and the monthly mean occurrence  
 805 frequency in spring are shown in Fig. S12a–c, respectively. The data points imply that the  
 806 vegetation growth rate does not affected the NPF spring characteristics. This could suggest that  
 807 a faster vegetation green-up, which is expectedly connected also to generally larger  
 808 concentrations of BVOCs, does not appear to influence the NPF occurrence.

809



823 **Figure 7.** Scatter plot of the start of spring date considering all vegetation and the start of NPF occurrence spring  
 824 season (peak). Labels for the measurement years Y1–Y8 and the calendar year of their spring (in brackets) are  
 825 also shown. The error bars indicate  $\pm 1$  SD. The solid red line represents the linear fit, while its dashed parts were  
 826 obtained by extrapolation. The data point for Y2 (2012) in black colour represents a forested environment, and,  
 827 therefore, it was excluded from the fitting. The coefficient of determination ( $R^2$ ) for the fit is also given. The line  
 828 of equality is displayed in black colour for orientating purpose.

#### 829 4 Conclusions

830 Annual mean NPF occurrence frequencies in a continental Central European area were  
 831 considerable (with an overall mean of 21 %), remained at a constant level (with an overall SD  
 832 of 5 %) and did not exhibit tendentious change over 2008–2018. The shapes of the distributions  
 833 of monthly mean occurrence frequency for the years varied substantially. The overall mean  
 834 distribution, however, possessed a pattern. Its structure was likely caused by multifactorial  
 835 influences of environmental properties. The most important components quantified in this  
 836 ambient study included gas-phase  $\text{H}_2\text{SO}_4$ ,  $\text{O}_3$ , GRad, WS, CS and RH. The factors also  
 837 involved precursor gases of vapours and their photochemical transformation processes.

838  
 839 A large fraction of chemical compounds contributing to NPF events in cities is expected to  
 840 originate from anthropogenic precursors. Their emissions may peak any time of year depending  
 841 on urban activities and human habits. Nevertheless, the  $f_{\text{NPF}}$  distributions seem to follow a  
 842 general spring maximum and winter minimum behaviour. This could be associated with a very  
 843 universal and widespread phenomenon. Emissions from vegetation or availability of (biogenic)  
 844 atmospheric chemical bases can be involved. We investigated here the role of some vegetation-

845 related factors in combination with environmental influencing properties in ambient NPF  
846 process. This approach represents a noteworthy novelty. We showed that there are several  
847 important links between the plant phenology in the area and event occurrence in spring as far  
848 as both their timing properties and some absolute measures/magnitudes are concerned. Tight  
849 pair wise relationships between  $f_{\text{NPF}}$  on one hand and a large variety of environmental variables  
850 on the other hand could not be, however, proved. This suggests that the environmental players  
851 comprising vegetation exert their impact in a joint manner as a sensitive outcome of interacting  
852 components.

853

854 The relationships between vegetation and NPF can further be investigated at a molecular level  
855 utilising long-term advanced/sophisticated on-line mass spectrometry of organic chemical  
856 species of vegetation origin among precursors, nucleating vapours and in molecular clusters.  
857 These measurements could also uncover additional links between vegetation and NPF events  
858 in summer and winter, which remained open questions in the present work. Understanding of  
859 these very complex and internally interacting multicomponent atmospheric chemical mixtures  
860 also requires complementing field and laboratory studies with modelling.

861 *Data availability.* The observational data are available from the corresponding author upon reasonable request.

862 *Supplement.* The supplement related to this article is available online.

863 *Author contributions.* IS designed and organised the research study. WT, PA, ZB and IS performed and assisted  
864 in most aerosol and meteorological measurements. WT accomplished most of the data treatment and prepared  
865 most figures. AK derived and evaluated the products from MODIS, temperature anomaly data and created the  
866 maps in Fig. 1. ZB calculated the Biome-BGCMuSo results. IS, MK, VMK, AK and ZB interpreted the results.  
867 IS wrote the manuscript with comments from all coauthors.

868 *Competing interests.* The authors declare that they have no conflict of interest.

869 *Acknowledgements.* The authors thank Z. Németh and T. Weidinger both of the Eötvös University for their  
870 assistance. We are grateful to L. Horváth and K. Labacz of the Hungarian Meteorological Service for providing  
871 the  $\text{NH}_3$  concentrations.

872 *Financial support.* This research has been supported by the Hungarian Research, Development and Innovation  
873 Office (grant nos. K116788, FK128709 and K132254), by the European Regional Development Fund and the  
874 Hungarian Government (GINOP-2.3.2-15-2016-00028), by the Advanced research supporting the forestry and  
875 wood-processing sector's adaptation to global change and the 4th industrial revolution (grant no.  
876 CZ.02.1.01/0.0/0.0/16\_019/0000803 financed by OP RDE), by the Academy of Finland (Center of Excellence in  
877 Atmospheric Sciences, grant no. 4100104), and by the ERC Advanced Grant ATM-GTP (grant no. 742206).

## 878 **References**

879 Almeida, J., Schobesberger, S., Kurten, A., Ortega, I. K., Kupiainen-Maatta, O., Praplan, A. P., Adamov, A.,  
880 Amorim, A., Bianchi, F., Breitenlechner, M., David, A., Dommen, J., Donahue, N. M., Downard, A., Dunne,  
881 E., Duplissy, J., Ehrhart, S., Flagan, R. C., Franchin, A., Guida, R., Hakala, J., Hansel, A., Heinritzi, M.,  
882 Henschel, H., Jokinen, T., Junninen, H., Kajos, M., Kangasluoma, J., Keskinen, H., Kupc, A., Kurten, T.,  
883 Kvashin, A. N., Laaksonen, A., Lehtipalo, K., Leiminger, M., Leppa, J., Loukonen, V., Makhmutov, V.,

884 Mathot, S., McGrath, M. J., Nieminen, T., Olenius, T., Onnela, A., Petäjä, T., Riccobono, F., Riipinen, I.,  
885 Rissanen, M., Rondo, L., Ruuskanen, T., Santos, F. D., Sarnela, N., Schallhart, S., Schnitzhofer, R.,  
886 Seinfeld, J. H., Simon, M., Sipilä, M., Stozhkov, Y., Stratmann, F., Tome, A., Tröstl, J., Tsagkogeorgas, G.,  
887 Vaattovaara, P., Viisanen, Y., Virtanen, A., Vrtala, A., Wagner, P. E., Weingartner, E., Wex, H.,  
888 Williamson, C., Wimmer, D., Ye, P. L., Yli-Juuti, T., Carslaw, K. S., Kulmala, M., Curtius, J.,  
889 Baltensperger, U., Worsnop, D. R., Vehkamäki, H., and Kirkby, J.: Molecular understanding of sulphuric  
890 acid–amine particle nucleation in the atmosphere, *Nature*, 502, 359–363,  
891 <https://doi.org/10.1038/nature12663>, 2013.

892 Baranzadeh, E., Arola, A., Hamed, A., Nieminen, T., Mikkonen, S., Virtanen, A., Kulmala, M., Lehtinen, K.,  
893 and Laaksonen, A.: The effect of cloudiness on new-particle formation: investigation of radiation levels,  
894 *Boreal Environ. Res.*, 19, 343–54, 2014.

895 Barcza, Z., Bondeau, A., Churkina, G., Ciais, Ph., Czóbel, Sz., Gelybó, Gy., Grosz, B., Haszpra, L., Hidy, D.,  
896 Horváth, L., Machon, A., Pásztor, L., Somogyi, Z., and Van Oost, K.: Modeling of biosphere-atmosphere  
897 exchange of greenhouse gases - Model based biospheric greenhouse gas balance of Hungary, in:  
898 *Atmospheric Greenhouse Gases: The Hungarian Perspective* (ed.: Haszpra, L.), Springer, Dordrecht, 295–  
899 330, [https://doi.org/10.1007/978-90-481-9950-1\\_13](https://doi.org/10.1007/978-90-481-9950-1_13), 2010.

900 Bianchi, F., Tröstl, J., Junninen, H., Frege, C., Henne, S., Hoyle, C. R., Molteni, U., Herrmann, E., Adamov, A.,  
901 Bukowiecki, N., Chen, X., Duplissy, J., Gysel, M., Hutterli, M., Kangasluoma, J., Kontkanen, J., Kürten, A.,  
902 Manninen, H. E., Münch, S., Peräkylä, O., Petäjä, T., Rondo, L., Williamson, C., Weingartner, E., Curtius, J.,  
903 Worsnop, D. R., Kulmala, M., Dommen, J., and Baltensperger, U.: New particle formation in the free  
904 troposphere: A question of chemistry and timing, *Science*, 352, 1109–1112,  
905 <https://doi.org/10.1126/science.aad5456>, 2016.

906 Birmili, W. and Wiedensohler, A.: New particle formation in the continental boundary layer: meteorological and  
907 gas phase parameter influence, *Geophys. Res. Lett.*, 27, 3325–3328, <https://doi.org/10.1029/1999GL011221>,  
908 2000.

909 Bonan, G.: *Ecological Climatology: concepts and applications*, Cambridge University Press, Cambridge,  
910 <https://doi.org/10.1017/CBO9781107339200>, 2015.

911 Bousiotis, D., Dall'Osto, M., Beddows, D. C. S., Pope, F. D., and Harrison, R. M.: Analysis of new particle  
912 formation (NPF) events at nearby rural, urban background and urban roadside sites, *Atmos. Chem. Phys.*, 19,  
913 5679–5694, <https://doi.org/10.5194/acp-19-5679-2019>, 2019.

914 Boy, M. and Kulmala, M.: Nucleation events in the continental boundary layer: Influence of physical and  
915 meteorological parameters, *Atmos. Chem. Phys.*, 2, 1–16, <https://doi.org/10.5194/acp-2-1-2002>, 2002.

916 Braakhuis, H. M., Park, M. V., Gosens, I., De Jong, W. H., and Cassee, F. R.: Physicochemical characteristics  
917 of nanomaterials that affect pulmonary inflammation, *Part. Fibre Toxicol.*, 11:18, <https://doi.org/10.1186/1743-8977-11-18>, 2014.

919 Brines, M., Dall'Osto, M., Beddows, D. C. S., Harrison, R. M., Gómez-Moreno, F., Núñez, L., Artíñano, B.,  
920 Costabile, F., Gobbi, G. P., Salimi, F., Morawska, L., Sioutas, C., and Querol, X.: Traffic and nucleation  
921 events as main sources of ultrafine particles in high-insolation developed world cities, *Atmos. Chem. Phys.*,  
922 15, 5929–5945, <https://doi.org/10.5194/acp-15-5929-2015>, 2015.

923 Carnerero, C., Pérez, N., Reche, C., Ealo, M., Titos, G., Lee, H.-K., Eun, H.-R., Park, Y.-H., Dada, L.,  
924 Paasonen, P., Kerminen, V.-M., Mantilla, E., Escudero, M., Gómez-Moreno, F. J., Alonso-Blanco, E., Coz,  
925 E., Saiz-Lopez, A., Temime-Roussel, B., Marchand, N., Beddows, D. C. S., Harrison, R. M., Petäjä, T.,  
926 Kulmala, M., Ahn, K.-H., Alastuey, A., and Querol, X.: Vertical and horizontal distribution of regional new  
927 particle formation events in Madrid, *Atmos. Chem. Phys.*, 18, 16601–16618, <https://doi.org/10.5194/acp-18-16601-2018>, 2018.

929 Carslaw, K. S., Lee, L. A., Reddington, C. L., Pringle, K. J., Rap, A., Forster, P. M., Mann, G. W., Spracklen,  
930 D. V., Woodhouse, M. T., Regayre, L. A., and Pierce, J. R.: Large contribution of natural aerosols to  
931 uncertainty in indirect forcing, *Nature*, 503, 67–71, <https://doi.org/10.1038/nature12674>, 2013.

932 Cornes, R., Van Der Schrier, G., Van Den Besselaar, E. J. M., and Jones, P. D.: An ensemble version of the E  
933 OBS temperature and precipitation datasets, *J. Geophys. Res. Atmos.*, 123, 9391–9409,  
934 <https://doi.org/10.1029/2017JD028200>, 2018.

935 Clement, C. F., Pirjola, L., Dal Maso, M., Mäkelä, J., and Kulmala, M.: Analysis of particle formation bursts  
936 observed in Finland, *J. Aerosol Sci.*, 32, 217–36, [https://doi.org/10.1016/S0021-8502\(00\)00059-8](https://doi.org/10.1016/S0021-8502(00)00059-8), 2001.

937 [Crouse, J. D., Nielsen, L. B., Jørgensen, S., Kjaergaard, H. G., and Wennberg, P. O.: Autoxidation of organic](https://doi.org/10.1021/jz4019207)  
938 [compounds in the atmosphere, \*J. Phys. Chem. Lett.\*, 4, 20, 3513–3520, <https://doi.org/10.1021/jz4019207>,](https://doi.org/10.1021/jz4019207)  
939 [2013.](https://doi.org/10.1021/jz4019207)

940 Dada, L., Paasonen, P., Nieminen, T., Buenrostro Mazon, S., Kontkanen, J., Peräkylä, O., Lehtipalo, K.,  
941 Hussein, T., Petäjä, T., Kerminen, V.-M., Bäck, J., and Kulmala, M.: Long-term analysis of clear-sky new  
942 particle formation events and nonevents in Hyytiälä, *Atmos. Chem. Phys.*, 17, 6227–6241,  
943 <https://doi.org/10.5194/acp-17-6227-2017>, 2017.

944 Dada, L., Ylivinkka, I., Baalbaki, R., Li, Ch., Guo, Y., Yan, Ch., Yao, L., Sarnela, N., Jokinen, T., Daellenbach,  
945 K. D., Yin, R., Deng, Ch., Chu, B., Nieminen, T., Kontkanen, J., Stolzenburg, D., Sipilä, M., Hussein, T.,  
946 Paasonen, P., Bianchi, F., Salma, I., Weidinger, T., Pikridas, M., Sciare, J., Jiang, J., Liu, Y., Petäjä, T.,  
947 Kerminen, V.-M., and Kulmala, M.: Sources and sinks driving sulphuric acid concentrations in contrasting  
948 environments: implications on proxy calculations, *Atmos. Chem. Phys.*, 20, 11747–11766,  
949 <https://doi.org/10.5194/acp-20-11747-2020>, 2020.

950 Dal Maso, M., Kulmala, M., Lehtinen, K. E. J., Mäkelä, J. M., Aalto, P. P., and O’Dowd, C.: Condensation and  
951 coagulation sinks and formation of nucleation mode particles in coastal and boreal forest boundary layers, *J.*  
952 *Geophys. Res.*, 107(19D), 8097, 10.1029/2001jd001053, 2002.

953 Dal Maso, M., Kulmala, M., Riipinen, I., Wagner, R., Hussein, T., Aalto, P. P., and Lehtinen, K. E. J.:  
954 Formation and growth of fresh atmospheric aerosols: eight years of aerosol size distribution data from  
955 SMEAR II, Hyytiälä, Finland, *Boreal Environ. Res.*, 10, 323–336, 2005.

956 Dall’Osto, M., Querol, X., Alastuey, A., O’Dowd, C., Harrison, R. M., Wenger, J., and Gómez-Moreno, F. J.: On  
957 the spatial distribution and evolution of ultrafine particles in Barcelona, *Atmos. Chem. Phys.*, 13, 741–759,  
958 <https://doi.org/10.5194/acp-13-741-2013>, 2013.

959 Dall’Osto, M., Beddows, D. C. S., Asmi, A., Poulain, L., Hao, L., Freney, E., Allan, J. D., Canagaratna, M.,  
960 Crippa, M., Bianchi, F., De Leeuw, G., Eriksson, A., Swietlicki, E., Hansson, H. C., Henzing, J. S., Granier,  
961 C., Zemankova, K., Laj, P., Onasch, T., Prevot, A., Putaud, J. P., Sellegri, K., Vidal, M., Virtanen, A., Simo,  
962 R., Worsnop, D., O’Dowd, C., Kulmala, M., and Harrison, R. M.: Novel insights on new particle formation  
963 derived from a pan-European observing system, *Sci. Reports*, 8, 1482, 01.12.2018,  
964 <https://doi.org/10.1038/s41598-017-17343-9>, 2018.

965 Dobor, L., Barcza, Z., Hlásny, T., Havasi, Á., Horváth, F., Ittész, P., and Bartholy, J.: Bridging the gap between  
966 climate models and impact studies: the FORESEE Database, *Geosci. Data J.*, 2, 1–11,  
967 <https://doi.org/10.1002/gdj3.22>, 2014.

968 Donahue, N. M., Ortega, I. K., Chuang, W., Riipinen, I., Riccobono, F., Schobesberger, S., Dommen, J.,  
969 Baltensperger, U., Kulmala, M., and Worsnop, D. R.: How do organic vapors contribute to new-particle  
970 formation?, *Faraday Discuss.*, 165, 91–104, <https://doi.org/10.1039/c3fd00046j>, 2013.

971 Dunne, E., Gordon, H., Kürten, A., Almeida, J., Duplissy, J., Williamson, Ch., Ortega, I., Pringle, K., Adamov,  
972 A., Baltensperger, U., Barmet, P., Benduhn, F., Bianchi, F., Breitenlechner, M., Clarke, A., Curtius, J.,  
973 Dommen, J., Donahue, N., Ehrhart, S., and Carslaw, K.: Global atmospheric particle formation from CERN  
974 CLOUD measurements, *Science*, 354, 10.1126/science.aaf2649, 2016.

975 Ehn, M., Thornton, J. A., Kleist, E., Sipilä, M., Junninen, H., Pullinen, I., Springer, M., Rubach, F., Tillmann,  
976 R., Lee, B., Lopez-Hilfiker, F., Andres, S., Acir, I. H., Rissanen, M., Jokinen, T., Schobesberger, S.,  
977 Kangasluoma, J., Kontkanen, J., Nieminen, T., Kurten, T., Nielsen, L. B., Jorgensen, S., Kjaergaard, H. G.,  
978 Canagaratna, M., Dal Maso, M., Berndt, T., Petäjä, T., Wahner, A., Kerminen, V. M., Kulmala, M.,  
979 Worsnop, D. R., Wildt, J., and Mentel, T. F.: A large source of low-volatility secondary organic aerosol,  
980 *Nature*, 506, 476–479, <https://doi.org/10.1038/nature13032>, 2014.

981 EMEP (Co-operative Programme for Monitoring and Evaluation of the Long-range Transmission of Air  
982 Pollutants in Europe) Manual, Chemical Co-ordination Centre Report 1/2002, Norwegian Institute for Air  
983 Research, Kjeller, 2002.

984 Erupe, M. E., Viggiano, A. A., and Lee, S.-H.: The effect of trimethylamine on atmospheric nucleation  
985 involving H<sub>2</sub>SO<sub>4</sub>, *Atmos. Chem. Phys.*, 11, 4767–4775, <https://doi.org/10.5194/acpd-10-27673-2010>, 2011.

986 Farquhar, G. D., von Caemmerer, S., and Berry, J. A.: A bio-chemical model of photosynthetic CO<sub>2</sub> assimilation  
987 in leaves of C3 species, *Planta*, 149, 78–90, <https://doi.org/10.1007/BF00386231>, 1980.

988 Frege, C., Ortega, I. K., Rissanen, M. P., Praplan, A. P., Steiner, G., Heinritzi, M., Ahonen, L., Amorim, A.,  
989 Bernhammer, A.-K., Bianchi, F., Brilke, S., Breitenlechner, M., Dada, L., Dias, A., Duplissy, J., Ehrhart, S.,  
990 El-Haddad, I., Fischer, L., Fuchs, C., Garmash, O., Gonin, M., Hansel, A., Hoyle, C. R., Jokinen, T.,  
991 Junninen, H., Kirkby, J., Kürten, A., Lehtipalo, K., Leiminger, M., Mauldin, R. L., Molteni, U., Nichman,  
992 L., Petäjä, T., Sarnela, N., Schobesberger, S., Simon, M., Sipilä, M., Stolzenburg, D., Tomé, A., Vogel, A.  
993 L., Wagner, A. C., Wagner, R., Xiao, M., Yan, C., Ye, P., Curtius, J., Donahue, N. M., Flagan, R. C.,  
994 Kulmala, M., Worsnop, D. R., Winkler, P. M., Dommen, J., and Baltensperger, U.: Influence of temperature  
995 on the molecular composition of ions and charged clusters during pure biogenic nucleation, *Atmos. Chem.*  
996 *Phys.*, 18, 65–79, <https://doi.org/10.5194/acp-18-65-2018>, 2018.

997 Gordon, H., Sengupta, K., Rap, A., Duplissy, J., Frege, C., Williamson, C., Heinritzi, M., Simon, M., Yan, C.,  
998 Almeida, J., Tröstl, J., Nieminen, T., Ortega, I. K., Wagner, R., Dunne, E. M., Adamov, A., Amorim, A.,  
999 Bernhammer, A. K., Bianchi, F., Breitenlechner, M., Brilke, S., Chen, X., Craven, J. S., Dias, A., Ehrhart, S.,  
1000 Fischer, L., Flagan, R. C., Franchin, A., Fuchs, C., Guida, R., Hakala, J., Hoyle, C. R., Jokinen, T., Junninen,  
1001 H., Kangasluoma, J., Kim, J., Kirkby, J., Krapf, M., Kürten, A., Laaksonen, A., Lehtipalo, K., Makhmutov,  
1002 V., Mathot, S., Molteni, U., Monks, S. A., Onnela, A., Peräkylä, O., Piel, F., Petäjä, T., Praplan, A. P.,  
1003 Pringle, K. J., Richards, N. A. D., Rissanen, M. P., Rondo, L., Sarnela, N., Schobesberger, S., Scott, C. E.,  
1004 Seinfeld, J. H., Sharma, S., Sipilä, M., Steiner, G., Stozhkov, Y., Stratmann, F., Tomé, A., Virtanen, A.,

- 1005 Vogel, A. L., Wagner, A. C., Wagner, P. E., Weingartner, E., Wimmer, D., Winkler, P. M., Ye, P., Zhang,  
1006 X., Hansel, A., Dommen, J., Donahue, N. M., Worsnop, D. R., Baltensperger, U., Kulmala, M., Curtius, J.,  
1007 and Carslaw, K. S.: Reduced anthropogenic aerosol radiative forcing caused by biogenic new particle  
1008 formation, *Proc. Natl. Acad. Sci. U.S.A.*, 113, 12053–12058, <https://doi.org/10.1073/pnas.1602360113>,  
1009 2016.
- 1010 [Guenther, A. B., Jiang, X., Heald, C. L., Sakulyanontvittaya, T., Duhl, T., Emmons, L. K., and Wang, X.: The](#)  
1011 [Model of Emissions of Gases and Aerosols from Nature, version 2.1 \(MEGAN2.1\): an extended and updated](#)  
1012 [framework for modeling biogenic emissions, \*Geosci. Model Dev.\*, 5, 1471–1492, \[https://doi.org/10.5194/gmd-5-\]\(https://doi.org/10.5194/gmd-5-1471-2012\)](#)  
1013 [1471-2012, 2012.](#)
- 1014 Hamed, A., Korhonen, H., Sihto, S.-L., Joutsensaari, J., Järvinen, H., Petäjä, T., Arnold, F., Nieminen, T.,  
1015 Kulmala, M., Smith, J. N., Lehtinen, K. E. J., and Laaksonen, A.: The role of relative humidity in continental  
1016 new particle formation. *J. Geophys. Res.*, 116, D03202, <https://doi.org/10.1029/2010JD014186>, 2011.
- 1017 He, X.-Ch., Tham, Y. J., Dada, L., Wang, M., Finkenzeller, H., Stolzenburg, D., Iyer, S., Simon, M., Shen, J.,  
1018 Rörup, B., Rissanen, M., Schobesberger, S., Baalbaki, R., Wang, D. S., Koenig, T. K., Jokinen, T., Sarnela,  
1019 N., Beck, L., Almeida, J., Kürten, A., Amanatidis, S., Amorim, A., Ataei, F., Baccharini, A., Bertozzi, B.,  
1020 Bianchi, F., Brilke, S., Caudillo, L., Chen, D., Chiu, R., Chu, B., Dias, A., Ding, A., Dommen, J., Duplissy,  
1021 J., El Haddad, I., Carracedo, L. G., Granzin, M., Hansel, A., Heinritzi, M., Hofbauer, V., Junninen, H.,  
1022 Kangasluoma, J., Kempainen, D., Kim, Ch., Kong, W., Krechmer, J. E., Kvashnin, A., Laitinen, T.,  
1023 Lamkaddam, H., Lee, Ch. P., Lehtipalo, K., Leiminger, M., Li, Z., Makhmutov, V., Manninen, H. E., Marie,  
1024 G., Marten, R., Mauldin, R. L., Mentler, B., Möhler, O., Müller, T., Nie, W., Onnela, A., Petäjä, T., Pfeifer,  
1025 J., Philippov, M., Ranjithkumar, A., Saiz-López, A., Salma, I., Scholz, W., Schuchmann, S., Schulze, B.,  
1026 Steiner, G., Stozhkov, Y., Tauber, Ch., Tomé, A., Thakur, R. C., Väisänen, O., Vazquez-Pufleau, M.,  
1027 Wagner, A. C., Wang, Y., Weber, S. K., Winkler, P. M., Wu, Y., Xiao, M., Yan, Ch., Ye, Q., Ylisirniö, A.,  
1028 Zauner-Wieczorek, M., Zha, Q., Zhou, P., Flagan, R. C., Curtius, J., Baltensperger, U., Kulmala, M.,  
1029 Kerminen, V.-M., Kurtén, T., Donahue, N. M., Volkamer, R., Kirkby, J., Worsnop, D. R., Sipilä, M.: Role  
1030 of iodine oxoacids in atmospheric aerosol nucleation, *Science*, accepted for publication,  
1031 <https://doi.org/10.5281/zenodo.4299441>, 2021.
- 1032 Heinritzi, M., Dada, L., Simon, M., Stolzenburg, D., Wagner, A. C., Fischer, L., Ahonen, L. R., Amanatidis, S.,  
1033 Baalbaki, R., Baccharini, A., Bauer, P. S., Baumgartner, B., Bianchi, F., Brilke, S., Chen, D., Chiu, R., Dias,  
1034 A., Dommen, J., Duplissy, J., Finkenzeller, H., Frege, C., Fuchs, C., Garmash, O., Gordon, H., Granzin, M.,  
1035 Haddad, I. E., He, X., Helm, J., Hofbauer, V., Hoyle, C. R., Kangasluoma, J., Keber, T., Kim, C., Kürten, A.,  
1036 Lamkaddam, H., Lampilahti, J., Laurila, T. M., Lee, C. P., Lehtipalo, K., Leiminger, M., Mai, H.,  
1037 Makhmutov, V., Manninen, H. E., Marten, R., Mathot, S., Mauldin, R. L., Mentler, B., Molteni, U., Müller,  
1038 T., Nie, W., Nieminen, T., Onnela, A., Partoll, E., Passananti, M., Petäjä, T., Pfeifer, J., Pospisilova, V.,  
1039 Quéléver, L., Rissanen, M. P., Rose, C., Schobesberger, S., Scholz, W., Scholze, K., Sipilä, M., Steiner, G.,  
1040 Stozhkov, Y., Tauber, C., Tham, Y. J., Vazquez-Pufleau, M., Virtanen, A., Vogel, A. L., Volkamer, R.,  
1041 Wagner, R., Wang, M., Weitz, L., Wimmer, D., Xiao, M., Yan, C., Ye, P., Zha, Q., Zhou, X., Amorim, A.,  
1042 Baltensperger, U., Hansel, A., Kulmala, M., Tomé, A., Winkler, P. M., Worsnop, D. R., Donahue, N. M.,  
1043 Kirkby, J., and Curtius, J.: Molecular understanding of the suppression of new-particle formation by  
1044 isoprene, *Atmos. Chem. Phys.*, 20, 11809–11821, <https://doi.org/10.5194/acp-20-11809-2020>, 2020.
- 1045 Hidy, D., Barcza, Z., Marjanović, H., Ostrogović Sever, M. Z., Dobor, L., Gelybó, G., Fodor, N., Pintér, K.,  
1046 Churkina, G., Running, S., Thornton, P., Bellocchi, G., Haszpra, L., Horváth, F., Suyker, A., and Nagy, Z.:  
1047 Terrestrial ecosystem process model Biome-BGCMuSo v4.0: summary of improvements and new modeling  
1048 possibilities, *Geosci. Model Dev.*, 9, 4405–4437, <https://doi.org/10.5194/gmd-9-4405-2016>, 2016.
- 1049 Hirsikko, A., Vakkari, V., Tiitta, P., Manninen, H. E., Gagné, S., Laakso, H., Kulmala, M., Mirme, A., Mirme,  
1050 S., Mabaso, D., Beukes, J. P., and Laakso, L.: Characterisation of sub-micron particle number concentrations  
1051 and formation events in the western Bushveld Igneous Complex, South Africa, *Atmos. Chem. Phys.*, 12,  
1052 3951–3967, <https://doi.org/10.5194/acp-12-3951-2012>, 2012.
- 1053 Hirsikko, A., Vakkari, V., Tiitta, P., Hatakka, J., Kerminen, V.-M., Sundström, A.-M., Beukes, J. P., Manninen,  
1054 H. E., Kulmala, M., and Laakso, L.: Multiple daytime nucleation events in semi-clean savannah and  
1055 industrial environments in South Africa: analysis based on observations, *Atmos. Chem. Phys.*, 13, 5523–  
1056 5532, 2013.
- 1057 Horváth, L., Fagerli, H., and Sutton, M. A.: Long-term record (1981–2005) of ammonia and ammonium  
1058 concentrations at K-puszta, Hungary and the effect of sulphur dioxide emission change on measured and  
1059 modelled concentrations, In: Sutton M. A., Reis S., and Baker S. M. (eds): *Atmospheric ammonia*. Springer,  
1060 Dordrecht, [https://doi.org/10.1007/978-1-4020-9121-6\\_12](https://doi.org/10.1007/978-1-4020-9121-6_12), 2009.
- 1061 [Jokinen, T., Sipilä, M., Junninen, H., Ehn, M., Lönn, G., Hakala, J., Petäjä, T., Mauldin III, R. L., Kulmala, M.,](#)  
1062 [and Worsnop, D. R.: Atmospheric sulphuric acid and neutral cluster measurements using CI-API-TOF,](#)  
1063 [Atmos. Chem. Phys., 12, 4117–4125, <https://doi.org/10.5194/acp-12-4117-2012>, 2012.](#)
- 1064 Jokinen, T., Berndt, T., Makkonen, R., Kerminen, V.-M., Junninen, H., Paasonen, P., Stratmann, F., Herrmann,  
1065 H., Guenther, A. B., Worsnop, D. R., Kulmala, M., Ehn, M. and Sipilä, M.: Production of extremely low

1066 volatile organic compounds from biogenic emissions: Measured yields and atmospheric implications, *Proc.*  
1067 *Natl. Acad. Sci. U.S.A.*, 112, 7123–7128, <https://doi.org/10.1073/pnas.1423977112>, 2015.

1068 Justice, C. O., Vermote, E., Townshend, J. R. G., Defries, R., Roy, D. P., Hall, D. K., Salomonson, V. V.,  
1069 Privette, J. L., Riggs, G., Strahler, A., Lucht, W., Myneni, R., Knjazihhin, Y., Running, S., Nemani, R.,  
1070 Wan, Z., Huete, A., vanLeeuwen, W., Wolfe, R., Giglio, L., Muller, J.-P., Lewis, P., and Barnsley, M.: The  
1071 Moderate Resolution Imaging Spectroradiometer (MODIS): land remote sensing for global change research,  
1072 *Trans. Geosci. Remote Sens.*, 36, 1228–1249, <https://doi.org/10.1109/36.701075>, 1998.

1073 Jun, Y.-S., Jeong, C.-H., Sabaliauskas, K., Leaitch, W. R., and Evans, G. J.: A year-long comparison of particle  
1074 formation events at paired urban and rural locations, *Atmos. Pollut. Res.*, 5, 447–54,  
1075 <https://doi.org/10.5094/APR.2014.052>, 2014.

1076 Kerminen, V.-M., Paramonov, M., Anttila, T., Riipinen, I., Fountoukis, C., Korhonen, H., Asmi, E., Laakso, L.,  
1077 Lihavainen, H., Swietlicki, E., Svenningsson, B., Asmi, A., Pandis, S. N., Kulmala, M., and Petäjä, T.:  
1078 Cloud condensation nuclei production associated with atmospheric nucleation: a synthesis based on existing  
1079 literature and new results, *Atmos. Chem. Phys.*, 12, 12037–12059, [https://doi.org/10.5194/acp-12-12037-](https://doi.org/10.5194/acp-12-12037-2012)  
1080 2012, 2012.

1081 Kerminen, V.-M., Chen, X., Vakkari, V., Petäjä, T., Kulmala, M., and Bianchi, F.: Atmospheric new particle  
1082 formation and growth: review of field observations, *Environ. Res. Lett.*, 13 (2018) 103003,  
1083 <https://doi.org/10.1088/1748-9326/aadf3c>, 2018.

1084 Kern, A., Marjanović, H., and Barcza, Z.: Evaluation of the quality of NDVI3g dataset against Collection 6  
1085 MODIS NDVI in Central-Europe between 2000 and 2013, *Remote Sens.*, 8, 955,  
1086 <https://doi.org/10.3390/rs8110955>, 2016.

1087 Kern, A., Marjanović, H., and Barcza, Z.: Spring vegetation green-up dynamics in Central Europe based on 20-  
1088 year long MODIS NDVI data, *Agric. For. Met.*, 287, 107969, <https://doi.org/10.1016/j.agrformet.2020.107969>,  
1089 2020.

1090 Kiendler-Scharr, A., Wildt, J., Dal Maso, M., Hohaus, T., Kleist, E., Mentel, T. F., Tillmann, R., Uerlings, R.,  
1091 Schurr, U., and Wahner, A.: New particle formation in forests inhibited by isoprene emissions, *Nature*, 461,  
1092 381–384, <https://doi.org/10.1038/nature08292>, 2009.

1093 Kirkby, J., Curtius, J., Almeida, J., Dunne, E., Duplissy, J., Ehrhart, S., Franchin, A., Gagné, S., Ickes, L.,  
1094 Kürten, A., Kupc, A., Metzger, A., Riccobono, F., Rondo, L., Schobesberger, S., Tsagkogeorgas, G.,  
1095 Wimmer, D., Amorim, A., Bianchi, F., Breitenlechner, M., David, A., Dommen, J., Downard, A., Ehn, M.,  
1096 Flagan, R. C., Haider, S., Hansel, A., Hauser, D., Jud, W., Junninen, H., Kreissl, F., Kvashin, A., Laaksonen,  
1097 A., Lehtipalo, K., Lima, J., Lovejoy, E. R., Makhutov, V., Mathot, S., Mikkilä, J., Minginette, P., Mogo, S.,  
1098 Nieminen, T., Onnela, A., Pereira, A., Petäjä, T., Schnitzhofer, R., Seinfeld, J. H., Sipilä, M., Stozhkov, Y.,  
1099 Stratmann, F., Tome, A., Vanhanen, J., Viisanen, J., Vrtala, A., Wagner, P. E., Walther, H., Weingartner, E.,  
1100 Wex, H., Winkler, P. M., Carslaw, K. S., Worsnop, D. R., Baltensperger, U., and Kulmala, M.: Role of  
1101 sulfuric acid, ammonia and galactic cosmic rays in atmospheric aerosol nucleation, *Nature*, 476, 429–433,  
1102 <https://doi.org/10.1038/nature10343>, 2011.

1103 Kirkby, J., Duplissy, J., Sengupta, K., Frege, C., Gordon, H., Williamson, C., Heinritzi, M., Simon, M., Yan, C.,  
1104 Almeida, J., Tröstl, J., Nieminen, T., Ortega, I. K., Wagner, R., Adamov, A., Amorim, A., Bernhammer, A.-  
1105 K., Bianchi, F., Breitenlechner, M., Brilke, S., Chen, X., Craven, J., Dias, A., Ehrhart, S., Flagan, R. C.,  
1106 Franchin, A., Fuchs, C., Guida, R., Hakala, J., Hoyle, C. R., Jokinen, T., Junninen, H., Kangasluoma, J.,  
1107 Kim, J., Krapf, M., Kürten, A., Laaksonen, A., Lehtipalo, K., Makhmutov, V., Mathot, S., Molteni, U.,  
1108 Onnela, A., Peräkylä, O., Piel, F., Petäjä, T., Praplan, A. P., Pringle, K., Rap, A., Richards, N. A. D.,  
1109 Riipinen, I., Rissanen, M. P., Rondo, L., Sarnela, N., Schobesberger, S., Scott, C. E., Seinfeld, J. H., Sipilä,  
1110 M., Steiner, G., Stozhkov, Y., Stratmann, F., Tomé, A., Virtanen, A., Vogel, A. L., Wagner, A., Wagner, P.  
1111 E., Weingartner, E., Wimmer, D., Winkler, P. M., Ye, P., Zhang, X., Hansel, A., Dommen, J., Donahue, N.  
1112 M., Worsnop, D. R., Baltensperger, U., Kulmala, M., Carslaw, K. S., and Curtius, J.: Ion-induced nucleation  
1113 of pure biogenic particles, *Nature*, 533, 521–526, <https://doi.org/10.1038/nature17953>, 2016.

1114 [Kontkanen, J., Paasonen, P., Aalto, J., Bäck, J., Rantala, P., Petäjä, T., and Kulmala, M.: Simple proxies for](https://doi.org/10.5194/acp-16-13291-2016)  
1115 [estimating the concentrations of monoterpenes and their oxidation products at a boreal forest site, \*Atmos.\*](https://doi.org/10.5194/acp-16-13291-2016)  
1116 [Chem. Phys.](https://doi.org/10.5194/acp-16-13291-2016), 16, 13291–13307, <https://doi.org/10.5194/acp-16-13291-2016>, 2016.

1117 Kulmala, M., Petäjä, T., Nieminen, T., Sipilä, M., Manninen, H. E., Lehtipalo, K., Dal Maso, M., Aalto, P. P.,  
1118 Junninen, H., Paasonen, P., Riipinen, I., Lehtinen, K. E. J., Laaksonen, A., and Kerminen, V.-M.:  
1119 Measurement of the nucleation of atmospheric aerosol particles, *Nat. Protoc.*, 7, 1651–1667,  
1120 <https://doi.org/10.1038/nprot.2012.091>, 2012.

1121 Kulmala, M., Kontkanen, J., Junninen, H., Lehtipalo, K., Manninen, H. E., Nieminen, T., Petäjä, T., Sipilä, M.,  
1122 Schobesberger, S., Rantala, P., Franchin, A., Jokinen, T., Järvinen, E., Äijälä, M., Kangasluoma, J., Hakala,  
1123 J., Aalto, P. P., Paasonen, P., Mikkilä, J., Vanhanen, J., Aalto, J., Hakola, H., Makkonen, U., Ruuskanen, T.,  
1124 Mauldin, R. L. III, Duplissy, J., Vehkamäki, H., Bäck, J., Kortelainen, A., Riipinen, I., Kurtén, T., Johnston,  
1125 M. V., Smith, J. N., Ehn, M., Mentel, T. F., Lehtinen, K. E. J., Laaksonen, A., Kerminen, V.-M., and

1126 Worsnop, D. R.: Direct observations of atmospheric aerosol nucleation, *Science*, 339, 943–946,  
1127 <https://doi.10.1126/science.1227385>, 2013.

1128 Kulmala, M., Petäjä, T., Ehn, M., Thornton, J., Sipilä, M., Worsnop, D. R., and Kerminen, V.-M.: Chemistry of  
1129 atmospheric nucleation: On the recent advances on precursor characterization and atmospheric cluster  
1130 composition in connection with atmospheric new particle formation, *Annu. Rev. Phys. Chem.*, 65, 21–37,  
1131 <https://doi.org/10.1146/annurev-physchem-040412-110014>, 2014.

1132 Kulmala, M., Kerminen, V. M., Petäjä, T., Ding, A. J., and Wang, L.: Atmospheric gas-to-particle conversion:  
1133 why NPF events are observed in megacities, *Faraday Discuss.*, <https://doi.10.1039/C6FD00257A>, 2017.

1134 Kürten, A.: New particle formation from sulfuric acid and ammonia: nucleation and growth model based on  
1135 thermodynamics derived from CLOUD measurements for a wide range of conditions, *Atmos. Chem. Phys.*,  
1136 19, 5033–5050, <https://doi.org/10.5194/acp-19-5033-2019>, 2019.

1137 Lee, S.-H., Gordon, H., Yu, H., Lehtipalo, K., Haley, R., Li, Y., and Zhang, R.: New particle formation in the  
1138 atmosphere: from molecular clusters to global climate, *J. Geophys. Res. Atmos.*, 124, 7098–7146,  
1139 <https://doi.org/10.1029/2018JD029356>, 2019.

1140 Lehtinen, K. E. J., Dal Maso, M., Kulmala, M., and Kerminen, V.-M.: Estimating nucleation rates from apparent  
1141 particle formation rates and vice versa: Revised formulation of the Kerminen-Kulmala equation, *J. Aerosol  
1142 Sci.*, 38, 988–994, <https://doi.org/10.1016/j.jaerosci.2007.06.009>, 2007.

1143 Lehtipalo, K., Rondo, L., Kontkanen, J., Schobesberger, S., Jokinen, T., Sarnela, N., Kürten, A., Ehrhart, S.,  
1144 Franchin, A., Nieminen, T., Riccobono, F., Sipilä, M., Yli-Juuti, T., Duplissy, J., Adamov, A., Ahlm, L.,  
1145 Almeida, J., Amorim, A., Bianchi, F., Breitenlechner, M., Dommen, J., Downard, A. J., Dunne, E. M.,  
1146 Flagan, R. C., Guida, R., Hakala, J., Hansel, A., Jud, W., Kangasluoma, J., Kerminen, V.-M., Keskinen, H.,  
1147 Kim, J., Kirkby, J., Kupc, A., Kupiainen-Määttä, O., Laaksonen, A., Lawler, M. J., Leiminger, M., Mathot,  
1148 S., Olenius, T., Ortega, I. K., Onnela, A., Petäjä, T., Praplan, A., Rissanen, M. P., Ruuskanen, T., Santos, F.  
1149 D., Schallhart, S., Schnitzhofer, R., Simon, M., Smith, J. N., Tröstl, J., Tsagkogeorgas, G., Tomé, A.,  
1150 Vaattovaara, P., Vehkamäki, H., Vrtala, A. E., Wagner, P. E., Williamson, C., Wimmer, D., Winkler, P. M.,  
1151 Virtanen, A., Donahue, N. M., Carslaw, K. S., Baltensperger, U., Riipinen, I., Curtius, J., Worsnop, D. R.  
1152 and Kulmala, M.: The effect of acid–base clustering and ions on the growth of atmospheric nano-particles,  
1153 *Nat. Commun.*, 7, 11594, <https://doi.org/10.1038/ncomms11594>, 2016.

1154 Lehtipalo, K., Yan, C., Dada, L., Bianchi, F., Xiao, M., Wagner, R., Stolzenburg, D., Ahonen, L. R., Amorim,  
1155 A., Baccarini, A., Bauer, P. S., Baumgartner, B., Bergen, A., Bernhammer, A.-K., Breitenlechner, M.,  
1156 Brilke, S., Buchholz, A., Mazon, S. B., Chen, D., Chen, X., Dias, A., Dommen, J., Draper, D. C., Duplissy,  
1157 J., Ehn, M., Finkenzeller, H., Fischer, L., Frege, C., Fuchs, C., Garmash, O., Gordon, H., Hakala, J., He, X.,  
1158 Heikkinen, L., Heinritzi, M., Helm, J. C., Hofbauer, V., Hoyle, C. R., Jokinen, T., Kangasluoma, J.,  
1159 Kerminen, V.-M., Kim, C., Kirkby, J., Kontkanen, J., Kürten, A., Lawler, M. J., Mai, H., Mathot, S.,  
1160 Mauldin, R. L., Molteni, U., Nichman, L., Nie, W., Nieminen, T., Ojdanic, A., Onnela, A., Passananti, M.,  
1161 Petäjä, T., Piel, F., Pospisilova, V., Quéléver, L. L. J., Rissanen, M. P., Rose, C., Sarnela, N., Schallhart, S.,  
1162 Schuchmann, S., Sengupta, K., Simon, M., Sipilä, M., Tauber, C., Tomé, A., Tröstl, J., Väisänen, O., Vogel,  
1163 A. L., Volkamer, R., Wagner, A. C., Wang, M., Weitz, L., Wimmer, D., Ye, P., Ylisirniö, A., Zha, Q.,  
1164 Carslaw, K. S., Curtius, J., Donahue, N. M., Flagan, R. C., Hansel, A., Riipinen, I., Virtanen, A., Winkler, P.  
1165 M., Baltensperger, U., Kulmala, M., and Worsnop, D. R.: Multicomponent new particle formation from  
1166 sulfuric acid, ammonia, and biogenic vapors, *Sci. Adv.*, 4, eaau5363, <https://doi.org/10.1126/sciadv.aau5363>,  
1167 2018.

1168 LP DAAC (Land Processes Distributed Active Archive Center), MOD09A1, Collection 6, NASA EOSDIS  
1169 Land Processes DAAC, USGS Earth Resources Observation and Science (EROS) Center, Sioux Falls, South  
1170 Dakota, 2019. URL: <https://lpdaac.usgs.gov>, accessed on 14 January 2020.

1171 Makkonen, R., Asmi, A., Korhonen, H., Kokkola, H., Järvenoja, S., Räisänen, P., Lehtinen, K. E. J., Laaksonen,  
1172 A., Kerminen, V.-M., Järvinen, H., Lohmann, U., Berrartz, R., Feichter, J., and Kulmala, M.: Sensitivity of  
1173 aerosol concentrations and cloud properties to nucleation and secondary organic distribution in ECHAM5-  
1174 HAM global circulation model, *Atmos. Chem. Phys.*, 9, 1747–1766, [https://doi.org/10.5194/acp-9-1747-  
1175 2009](https://doi.org/10.5194/acp-9-1747-2009), 2009.

1176 Makkonen, R., Asmi, A., Kerminen, V.-M., Boy, M., Arneth, A., Hari, P., and Kulmala, M.: Air pollution  
1177 control and decreasing new particle formation lead to strong climate warming, *Atmos. Chem. Phys.*, 12,  
1178 1515–1524, <https://doi.10.5194/acpd-11-25991-2011>, 2012.

1179 Manninen, H. E., Nieminen, T., Asmi, E., Gagné, S., Häkkinen, S., Lehtipalo, K., Aalto, P., Vana, M., Mirme,  
1180 A., Mirme, S., Hörrak, U., Plass-Dülmer, C., Stange, G., Kiss, G., Hoffer, A., Törö, N., Moerman, M.,  
1181 Henzig, B., de Leeuw, G., Brinkenberg, M., Kouvarakis, G. N., Bougiatioti, A., Mihalopoulos, N.,  
1182 O’Dowd, C., Ceburnis, D., Arneth, A., Svenningsson, B., Swietlicki, E., Tarozzi, L., Decesari, S., Facchini,  
1183 M. C., Birmili, W., Sonntag, A., Wiedensohler, A., Boulon, J., Sellegri, K., Laj, P., Gysel, M., Bukowiecki,  
1184 N., Weingartner, E., Wehrle, G., Laaksonen, A., Hamed, A., Joutsensaari, J., Petäjä, T., Kerminen, V.-M., and  
1185 Kulmala, M.: EUCAARI ion spectrometer measurements at 12 European sites – analysis of new particle  
1186 formation events, *Atmos. Chem. Phys.*, 10, 7907–7927, <https://doi.org/10.5194/acp-10-7907-2010>, 2010.



1187 McFiggans, G., Mentel, T. F., Wildt, J., Pullinen, I., Kang, S., Kleist, E., Schmitt, S., Springer, M., Tillmann, R.,  
1188 Wu, C., Zhao, D., Hallquist, M., Faxon, C., Le Breton, M., Hallquist, A. M., Simpson, D., Bergstroem, R.,  
1189 Jenkin, M. E., Ehn, M., Thornton, J. A., Alfarra, M. R., Bannan, T. J., Percival, C. J., Priestley, M., Topping,  
1190 D., and Kiendler-Scharr, A.: Secondary organic aerosol reduced by mixture of atmospheric vapours, *Nature*,  
1191 565, 587–593, <https://doi.org/10.1038/s41586-018-0871-y>, 2019.

1192 Meija, J. F. and Morawska, L.: An investigation of nucleation events in a coastal urban environment in the  
1193 Southern Hemisphere, *Atmos. Chem. Phys.*, 9, 7877–7888, <https://doi.org/10.5194/acp-9-7877-2009>, 2009.

1194 Merikanto, J., Spracklen, D. V., Mann, G. W., Pickering, S. J., and Carslaw, K. S.: Impact of nucleation on  
1195 global CCN, *Atmos. Chem. Phys.*, 9, 8601–8616, <https://doi.org/10.5194/acp-9-8601-2009>, 2009.

1196 Metzger, A., Verheggen, B., Dommen, J., Duplissy, J., Prévôt, A. S. H., Weingartner, E., Riipinen, I., Kulmala,  
1197 M., Spracklen, D. V., Carslaw, K. S., and Baltensperger, U.: Evidence for the role of organics in aerosol  
1198 particle formation under atmospheric conditions, *Proc. Natl. Acad. Sci. U. S. A.*, 107, 6646–6651,  
1199 <https://doi.org/10.1073/pnas.0911330107>, 2010.

1200 Mikkonen, S., Lehtinen, K. E. J., Hamed, A., Joutsensaari, J., Facchini, M. C., and Laaksonen, A.: Using  
1201 discriminant analysis as a nucleation event classification method, *Atmos. Chem. Phys.*, 6, 5549–5557,  
1202 <https://doi.org/10.5194/acp-6-5549-2006>, 2006.

1203 Mikkonen, S., Németh, Z., Varga, V., Weidinger, T., Leinonen, V., Yli-Juuti, T., and Salma, I.: Decennial time  
1204 trends and diurnal patterns of particle number concentrations in a Central European city between 2008 and  
1205 2018, *Atmos. Chem. Phys.*, 20, 12247–12263, <https://doi.org/10.5194/acp-20-12247-2020>, 2020.

1206 Mozurkewich, M.: The dissociation constant of ammonium nitrate and its dependence on temperature, relative  
1207 humidity and particle size, *Atmos. Environ.*, 27A, 261–270, [https://doi.org/10.1016/0960-1686\(93\)90356-4](https://doi.org/10.1016/0960-1686(93)90356-4),  
1208 1993.

1209 Németh, Z. and Salma, I.: Spatial extension of nucleating air masses in the Carpathian Basin, *Atmos. Chem.*  
1210 *Phys.*, 14, 8841–8848, <https://doi.org/10.5194/acp-14-8841-2014>, 2014.

1211 Németh, Z., Rosati, B., Zíková, N., Salma, I., Bozó, L., Dameto de España, C., Schwarz, J., Ždímal, V., and  
1212 Wonaschütz, A.: Comparison of atmospheric new particle formation and growth events in three Central  
1213 European cities, *Atmos. Environ.*, 178, 191–197, <https://doi.org/10.1016/j.atmosenv.2018.01.035>, 2018.

1214 Nenes, A., Pandis, S. N., Weber, R. J., and Russell, A.: Aerosol pH and liquid water content determine when  
1215 particulate matter is sensitive to ammonia and nitrate availability, *Atmos. Chem. Phys.*, 20, 3249–3258,  
1216 <https://doi.org/10.5194/acp-20-3249-2020>, 2020.

1217 Nieminen, T., Asmi, A., Dal Maso, M., P. Aalto, P., Keronen, P., Petäjä, T., Kulmala, M., and Kerminen, V.-M.:  
1218 Trends in atmospheric new-particle formation: 16 years of observations in a boreal-forest environment,  
1219 *Boreal Env. Res.*, 19 (suppl. B), 191–214, 2014.

1220 Nieminen, T., Kerminen, V.-M., Petäjä, T., Aalto, P. P., Arshinov, M., Asmi, E., Baltensperger, U., Beddows,  
1221 D. C. S., Beukes, J. P., Collins, D., Ding, A., Harrison, R. M., Henzing, B., Hooda, R., Hu, M., Hörrak, U.,  
1222 Kivekäs, N., Komsaare, K., Krejčí, R., Kristensson, A., Laakso, L., Laaksonen, A., Leaitch, W. R.,  
1223 Lihavainen, H., Mihalopoulos, N., Németh, Z., Nie, W., O'Dowd, C., Salma, I., Sellegri, K., Svenningsson,  
1224 B., Swietlicki, E., Tunved, P., Ulevicius, V., Vakkari, V., Vana, M., Wiedensohler, A., Wu, Z., Virtanen, A.,  
1225 and Kulmala, M.: Global analysis of continental boundary layer new particle formation based on long-term  
1226 measurements, *Atmos. Chem. Phys.*, 18, 14737–14756, <https://doi.org/10.5194/acp-18-14737-2018>, 2018.

1227 O'Dowd, C. D., Jimenez, J. L., Bahreini, R., Flagan, R. C., Seinfeld, J. H., Hämeri, K., Pirjola, L., Kulmala, M.,  
1228 Jennings, S. G., and Hoffmann, Th.: Marine aerosol formation from biogenic iodine emissions, *Nature* 417,  
1229 632–636, <https://doi.org/10.1038/nature00775>, 2002.

1230 Ohlwein, S., Kappeler, R., Joss, M. K., Künzli, N., and Hoffmann, B.: Health effects of ultrafine particles: a  
1231 systematic literature review update of epidemiological evidence, *Int. J. Public Health*, 685, 547–559,  
1232 <https://doi.org/10.1007/s00038-019-01202-7>, 2019.

1233 Petäjä, T., Mauldin, III, R. L., Kosciuch, E., McGrath, J., Nieminen, T., Paasonen, P., Boy, M., Adamov, A.,  
1234 Kotiaho, T., and Kulmala, M.: Sulfuric acid and OH concentrations in a boreal forest site, *Atmos. Chem.*  
1235 *Phys.*, 9, 7435–7448, <https://doi.org/10.5194/acp-9-7435-2009>, 2009.

1236 Qian, S., Sakurai, H., and McMurry, P. H.: Characteristics of regional nucleation events in urban East St. Louis,  
1237 *Atmos. Environ.* 41 4119–4127, <https://doi.org/10.1016/j.atmosenv.2007.01.011>, 2007.

1238 Riccobono, F., Schobesberger, S., Scott, C., Dommen, J., Ortega, I., Rondo, L., Almeida, J., Amorim, A.,  
1239 Bianchi, F., Breitenlechner, M., David, A., Downard, A., Dunne, E., Duplissy, J., Ehrhart, S., Flagan, R.,  
1240 Franchin, A., Hansel, A., Junninen, H., Kajos, M., Keskinen, H., Kupc, A., Kurten, A., Kvashin, A.,  
1241 Laaksonen, A., Lehtipalo, K., Makhmutov, V., Mathot, S., Nieminen, T., Onnela, A., Petäjä, T., Praplan, A.,  
1242 Santos, F., Schallhart, S., Seinfeld, J., Sipilä, M., Spracklen, D., Stozhkov, Y., Stratmann, F., Tome, A.,  
1243 Tsagkogeorgas, G., Vaattovaara, P., Viisanen, Y., Vrtala, A., Wagner, P., Weingartner, E., Wex, H.,  
1244 Wimmer, D., Carslaw, K., Curtius, J., Donahue, N., Kirkby, J., Kulmala, M., Worsnop, D., and  
1245 Baltensperger, U.: Oxidation products of biogenic emissions contribute to nucleation of atmospheric  
1246 particles, *Science*, 344, 717–721, <https://doi.org/10.1126/science.1243527>, 2014.

1247 Riipinen, I., Pierce, J. R., Yli-Juuti, T., Nieminen, T., Häkkinen, S., Ehn, M., Junninen, H., Lehtipalo, K., Petäjä,  
1248 T., Slowik, J., Chang, R., Shantz, N. C., Abbatt, J., Leaitch, W. R., Kerminen, V.-M., Worsnop, D. R.,  
1249 Pandis, S. N., Donahue, N. M., and Kulmala, M.: Organic condensation: a vital link connecting aerosol  
1250 formation to cloud condensation nuclei (CCN) concentrations, *Atmos. Chem. Phys.*, 11, 3865–3878,  
1251 <https://doi.org/10.5194/acp-11-3865-2011>, 2011.

1252 Rouse, J. W., Haas, R. H., Deering, D. W., Schell, J. A., and Harlan, J. C.: Monitoring the vernal advancement  
1253 and retrogradation (green wave effect) of natural vegetation, NASA/GSFC Type III Final Report, Greenbelt,  
1254 MD., pp. 371, 1974.

1255 Salma, I. and Németh, Z.: Dynamic and timing properties of new aerosol particle formation and consecutive  
1256 growth events, *Atmos. Chem. Phys.*, 19, 5835–5852, <https://doi.org/10.5194/acp-19-5835-2019>, 2019.

1257 Salma, I., Borsós, T., Weidinger, T., Aalto, P., Hussein, T., Dal Maso, M., and Kulmala, M.: Production, growth  
1258 and properties of ultrafine atmospheric aerosol particles in an urban environment, *Atmos. Chem. Phys.*, 11,  
1259 1339–1353, <https://doi.org/10.5194/acp-11-1339-2011>, 2011.

1260 Salma, I., Borsós, T., Németh, Z., Weidinger, T., Aalto, T., and Kulmala, M.: Comparative study of ultrafine  
1261 atmospheric aerosol within a city, *Atmos. Environ.*, 92, 154–161,  
1262 <https://doi.org/10.1016/j.atmosenv.2014.04.020>, 2014.

1263 Salma, I., Füre, P., Németh, Z., Farkas, Á., Balásházy, I., Hofmann, W., and Farkas, Á.: Lung burden and  
1264 deposition distribution of inhaled atmospheric urban ultrafine particles as the first step in their health risk  
1265 assessment, *Atmos. Environ.*, 104, 39–49, <https://doi.org/10.1016/j.atmosenv.2014.12.060>, 2015.

1266 Salma, I., Németh, Z., Weidinger, T., Kovács, B., and Kristóf, G.: Measurement, growth types and shrinkage of  
1267 newly formed aerosol particles at an urban research platform, *Atmos. Chem. Phys.*, 16, 7837–7851,  
1268 <https://doi.org/10.5194/acp-16-7837-2016>, 2016a.

1269 Salma, I., Németh, Z., Kerminen, V. M., Aalto, P., Nieminen, T., Weidinger, T., Molnár, Á., Imre, K., and  
1270 Kulmala, M.: Regional effect on urban atmospheric nucleation, *Atmos. Chem. Phys.*, 16, 8715–8728,  
1271 <https://doi.org/10.5194/acp-16-8715-2016>, 2016b.

1272 Salma, I., Varga, V., and Németh, Z.: Quantification of an atmospheric nucleation and growth process as a  
1273 single source of aerosol particles in a city, *Atmos. Chem. Phys.*, 17, 15007–15017,  
1274 <https://doi.org/10.5194/acp-17-15007-2017>, 2017.

1275 Salma, I., Vasánits-Zsigrai, A., Machon, A., Varga, T., Major, I., Gergely, V., and Molnár, M.: Fossil fuel  
1276 combustion, biomass burning and biogenic sources of fine carbonaceous aerosol in the Carpathian Basin,  
1277 *Atmos. Chem. Phys.*, 20, 4295–4312, <https://doi.org/10.5194/acp-20-4295-2020>, 2020.

1278 Schobesberger, S., Junninen, H., Bianchi, F., Lonn, G., Ehn, M., Lehtipalo, K., Dommen, J., Ehrhart, S., Ortega,  
1279 I. K., Franchin, A., Nieminen, T., Riccobono, F., Hutterli, M., Duplissy, J., Almeida, J., Amorim, A.,  
1280 Breitenlechner, M., Downard, A. J., Dunne, E. M., Flagan, R. C., Kajos, M., Keskinen, H., Kirkby, J., Kupc,  
1281 A., Kurten, A., Kurten, T., Laaksonen, A., Mathot, S., Onnela, A., Praplan, A. P., Rondo, L., Santos, F. D.,  
1282 Schallhart, S., Schnitzhofer, R., Sipilä, M., Tome, A., Tsagkogeorgas, G., Vehkamäki, H., Wimmer, D.,  
1283 Baltensperger, U., Carslaw, K. S., Curtius, J., Hansel, A., Petäjä, T., Kulmala, M., Donahue, N. M., and  
1284 Worsnop, D. R.: Molecular understanding of atmospheric particle formation from sulfuric acid and large  
1285 oxidized organic molecules, *Proc. Natl. Acad. Sci. U.S.A.*, 110, 17223–17228,  
1286 <https://doi.org/10.1073/pnas.1306973110>, 2013.

1287 Shen, M., Piao, S., Cong, N., Zhang, G., and Jassens, I. A.: Precipitation impacts on vegetation spring  
1288 phenology on the Tibetan Plateau, *Glob. Chang. Biol.*, 21, 3647–3656, <https://doi.org/10.1111/gcb.12961>,  
1289 2015.

1290 Seyednasrollah, B., Swenson, J. J., Domec, J. C., and Clark, J. S.: Leaf phenology paradox: Why warming  
1291 matters most where it is already warm, *Remote Sens. Environ.*, 209, 446–455,  
1292 <https://doi.org/10.1016/j.rse.2018.02.059>, 2018.

1293 Sihto, S.-L., Kulmala, M., Kerminen, V.-M., Dal Maso, M., Petäjä, T., Riipinen, I., Korhonen, H., Arnold, F.,  
1294 Janson, R., Boy, M., Laaksonen, A., and Lehtinen, K. E. J.: Atmospheric sulphuric acid and aerosol  
1295 formation: implications from atmospheric measurements for nucleation and early growth mechanisms,  
1296 *Atmos. Chem. Phys.*, 6, 4079–4091, <https://doi.org/10.5194/acp-6-4079-2006>, 2006.

1297 Sihto, S.-L., Mikkilä, J., Vanhanen, J., Ehn, M., Liao, L., Lehtipalo, K., Aalto, P. P., Duplissy, J., Petäjä, T.,  
1298 Kerminen, V.-M., Boy, M., and Kulmala, M.: Seasonal variation of CCN concentrations and aerosol  
1299 activation properties in boreal forest, *Atmos. Chem. Phys.*, 11, 13269–13285, <https://doi.org/10.5194/acp-11-13269-2011>, 2011.

1300 Simon, M., Dada, L., Heinritzi, M., Scholz, W., Stolzenburg, D., Fischer, L., Wagner, A. C., Kürten, A., Rörup,  
1301 B., He, X.-C., Almeida, J., Baalbaki, R., Baccarini, A., Bauer, P. S., Beck, L., Bergen, A., Bianchi, F.,  
1302 Bräkling, S., Brilke, S., Caudillo, L., Chen, D., Chu, B., Dias, A., Draper, D. C., Duplissy, J., El Haddad, I.,  
1303 Finkenzeller, H., Frege, C., Gonzalez-Carracedo, L., Gordon, H., Granzin, M., Hakala, J., Hofbauer, V.,  
1304 Hoyle, C. R., Kim, C., Kong, W., Lamkaddam, H., Lee, C. P., Lehtipalo, K., Leiminger, M., Mai, H.,  
1305 Manninen, H. E., Marie, G., Marten, R., Mentler, B., Molteni, U., Nichman, L., Nie, W., Ojdanic, A.,  
1306 Onnela, A., Partoll, E., Petäjä, T., Pfeifer, J., Philippov, M., Quéléver, L. L. J., Ranjithkumar, A., Rissanen,  
1307

1308 M., Schallhart, S., Schobesberger, S., Schuchmann, S., Shen, J., Sipilä, M., Steiner, G., Stozhkov, Y.,  
1309 Tauber, C., Tham, Y. J., Tomé, A. R., Vazquez-Pufleau, M., Vogel, A., Wagner, R., Wang, M., Wang, D. S.,  
1310 Wang, Y., Weber, S. K., Wu, Y., Xiao, M., Yan, C., Ye, P., Ye, Q., Zauner-Wieczorek, M., Zhou, X.,  
1311 Baltensperger, U., Dommen, J., Flagan, R. C., Hansel, A., Kulmala, M., Volkamer, R., Winkler, P. M.,  
1312 Worsnop, D. R., Donahue, N. M., Kirkby, J., and Curtius, J.: Molecular understanding of new-particle  
1313 formation from alpha-pinene between  $-50\text{ }^{\circ}\text{C}$  and  $25\text{ }^{\circ}\text{C}$ , *Atmos. Chem. Phys.*, 20, 9183–9207,  
1314 <https://doi.org/10.5194/acp-20-9183-2020>, 2020.

1315 Sipilä, M., Berndt, T., Petäjä, T., Brus, D., Vanhanen, J., Stratmann, F., Patokoski, J., Mauldin, R. L. 3rd,  
1316 Hyvärinen, A. P., Lihavainen, H., and Kulmala, M.: The role of sulfuric acid in atmospheric nucleation,  
1317 *Science*, 327, 1243–1246, <https://doi.10.1126/science.1180315>, 2010.

1318 Sipilä, M., Sarnela, N., Jokinen, T., Henschel, H., Junninen, H., Kontkanen, J., Richters, S., Kangasluoma, J.,  
1319 Franchin, A., Peräkylä, O., Rissanen, M. P., Ehn, M., Vehkamäki, H., Kurten, T., Berndt, T., Petäjä, T.,  
1320 Worsnop, D., Ceburnis, D., Kerminen, V.-M., Kulmala, M., and O'Dowd, C.: Molecular-scale evidence of  
1321 aerosol particle formation via sequential addition of  $\text{HIO}_3$ , *Nature*, 537, 532–534,  
1322 <https://doi.org/10.1038/nature19314>, 2016.

1323 Spracklen, D. V., Carslaw, K. S., Merikanto, J., Mann, G. W., Reddington, C. L., Pickering, S., Ogren, J. A.,  
1324 Andrews, E., Baltensperger, U., Weingartner, E., Boy, M., Kulmala, M., Laakso, L., Lihavainen, H.,  
1325 Kivekäs, N., Komppula, M., Mihalopoulos, N., Kouvarakis, G., Jennings, S. G., O'Dowd, C., Birmili, W.,  
1326 Wiedensohler, A., Weller, R., Gras, J., Laj, P., Sellegri, K., Bonn, B., Krejčí, R., Laaksonen, A., Hamed, A.,  
1327 Minikin, A., Harrison, R. M., Talbot, R., and Sun, J.: The contribution of boundary layer nucleation events  
1328 to total particle concentrations on regional and global scales, *Atmos. Chem. Phys.*, 6, 5631–5648,  
1329 <https://doi.org/10.5194/acp-6-5631-2006>, 2006.

1330 Sulla-Menashe, D. and Friedl, M. A.: User guide to collection 6 MODIS land cover (MCD12Q1 and  
1331 MCD12C1) product, Available online: [https://lpdaac.usgs.gov/sites/default/files/public/  
1332 product\\_documentation/mcd12\\_user\\_guide\\_v6.pdf](https://lpdaac.usgs.gov/sites/default/files/public/product_documentation/mcd12_user_guide_v6.pdf), 2018.

1333 Sun, J., Birmili, W., Hermann, M., Tuch, T., Weinhold, K., Spindler, G., Schladitz, A., Bastian, S., Löschau, G.,  
1334 Cyrus, J., Gu, J., Flentje, H., Briel, B., Asbach, C., Kaminski, H., Ries, L., Sohmer, R., Gerwig, H., Wirtz,  
1335 K., Meinhardt, F., Schwerin, A., Bath, O., Ma, N., and Wiedensohler, A.: Variability of Black Carbon mass  
1336 concentrations, sub-micrometer particle number concentrations and size distributions: Results of the German  
1337 Ultrafine Aerosol Network ranging from city street to high Alpine locations, *Atmos. Environ.*, 202, 256–268,  
1338 <https://doi.org/10.1016/j.atmosenv.2018.12.029>, 2019.

1339 [Taipale, R., Ruuskanen, T. M., Rinne, J., Kajos, M. K., Hakola, H., Pohja, T. and Kulmala, M.: Technical Note: Quantitative long-term measurements of VOC concentrations by PTR-MS – measurement, calibration, and volume mixing ratio calculation methods, \*Atmos. Chem. Phys.\*, 8, 6681–6698, doi:10.5194/acp-8-6681-2008, 2008](#)

1343 Thornton, P. E. and Rosenbloom, N. A.: Ecosystem model spin-up: Estimating steady state conditions in a  
1344 coupled terrestrial carbon and nitrogen cycle model, *Ecol. Model.*, 189, 25–48,  
1345 <https://doi.org/10.1016/j.ecolmodel.2005.04.008>, 2005.

1346 Tröstl, J., Chuang, W. K., Gordon, H., Heinritzi, M., Yan, C., Molteni, U., Ahlm, L., Frege, C., Bianchi, F.,  
1347 Wagner, R., Simon, M., Lehtipalo, K., Williamson, C., Craven, J. S., Duplissy, J., Adamov, A., Almeida, J.,  
1348 Bernhammer, A. K., Breitenlechner, M., Brilke, S., Dias, A., Ehrhart, S., Flagan, R. C., Franchin, A., Fuchs,  
1349 C., Guida, R., Gysel, M., Hansel, A., Hoyle, C. R., Jokinen, T., Junninen, H., Kangasluoma, J., Keskinen,  
1350 H., Kim, J., Krapf, M., Kürten, A., Laaksonen, A., Lawler, M., Leiminger, M., Mathot, S., Möhler, O.,  
1351 Nieminen, T., Onnela, A., Petäjä, T., Piel, F. M., Miettinen, P., Rissanen, M. P., Rondo, L., Sarnela, N.,  
1352 Schobesberger, S., Sengupta, K., Sipilä, M., Smith, J. N., Steiner, G., Tomé, A., Virtanen, A., Wagner, A.  
1353 C., Weingartner, E., Wimmer, D., Winkler, P. M., Ye, P. L., Carslaw, K. S., Curtius, J., Dommen, J., Kirkby,  
1354 J., Kulmala, M., Riipinen, I., Worsnop, D. R., Donahue, N. M., and Baltensperger, U.: The role of low-  
1355 volatility organic compounds in initial particle growth in the atmosphere, *Nature*, 533, 527,  
1356 [10.1038/nature18271](https://doi.org/10.1038/nature18271), 2016.

1357 Tunved, P., Hansson, H.-C., Kerminen, V.-M., Ström, J., Dal Maso, M., Lihavainen, H., Viisanen, Y., Aalto, P.  
1358 P., Komppula, M., and Kulmala, M.: High natural aerosol loading over boreal forest, *Science*, 312, 261–263,  
1359 <https://doi.10.1126/science.1123052>, 2006.

1360 Vakkari, V., Laakso, H., Kulmala, M., Laaksonen, A., Mabaso, D., Molefe, M., Kgabi, N., and Laakso, L.: New  
1361 particle formation events in semi-clean South African savannah, *Atmos. Chem. Phys.*, 11, 3333–3346,  
1362 <https://doi.10.5194/acp-11-3333-2011>, 2011.

1363 Vermote, E.: MOD09A1 MODIS/Terra Surface Reflectance 8-Day L3 Global 500 m SIN Grid V006, NASA  
1364 EOSDIS Land Processes DAAC, 2015, accessed on 23 May 2018,  
1365 <https://doi.10.5067/MODIS/MOD09A1.006>.

1366 Wu, Z., Hu, M., Liu, S., Wehner, B., Bauer, S., Massling, A., Wiedensohler, A., Petäjä, T., Dal Maso, M. and  
1367 Kulmala, M.: New particle formation in Beijing, China: statistical analysis of a 1 year data set, *J. Geophys.  
1368 Res.*, 112, D09209, <https://doi.10.1029/2006JD007406>, 2007.

1369 Xiao, S., Wang, M. Y., Yao, L., Kulmala, M., Zhou, B., Yang, X., Chen, J. M., Wang, D. F., Fu, Q. Y.,  
1370 Worsnop, D. R., and Wang, L.: Strong atmospheric new particle formation in winter in urban Shanghai,  
1371 China, *Atmos. Chem. Phys.*, 15, 1769–1781, <https://doi.org/10.5194/acp-15-1769-2015>, 2015.  
1372 Yao, L., Garmash, O., Bianchi, F., Zheng, J., Yan, C., Kontkanen, J., Junninen, H., Mazon, S. B., Ehn, M.,  
1373 Paasonen, P., Sipilä, M., Wang, M., Wang, X., Xiao, S., Chen, H., Lu, Y., Zhang, B., Wang, D., Fu, Q.,  
1374 Geng, F., Li, L., Wang, H., Qiao, L., Yang, X., Chen, J., Kerminen, V.-M., Petäjä, T., Worsnop, D. R.,  
1375 Kulmala, M., and Wang, L.: Atmospheric new particle formation from sulfuric acid and amines in a Chinese  
1376 megacity, *Science*, 361, 278–281, <https://doi.10.1126/science.aao4839>, 2018.  
1377 Yue, D. L., Hu, M., Zhang, R. Y., Wang, Z. B., Zheng, J., Wu, Z. J., Wiedensohler, A., He, L. Y., Huang, X. F.,  
1378 and Zhu, T.: The roles of sulfuric acid in new particle formation and growth in the mega-city of Beijing,  
1379 *Atmos. Chem. Phys.*, 10, 4953–4960, <https://doi.10.5194/acp-10-4953-2010>, 2010.  
1380 Zhao, S., Yu, Y., Yin, D., and He, J.: Meteorological dependence of particle number concentrations in an urban  
1381 area of complex terrain, *Atmos. Res.*, 164–165, 304–305, <https://doi.org/10.1016/j.atmosres.2015.06.001>,  
1382 2015